LA-UR-99-5329

Title: ***Urban parameterizations for mesoscale meteorological models***

Author: ***Michael J. Brown***
Energy and Environmental Analysis (TSA-4)

Submitted to: ***Mesoscale Atmospheric Dispersion, Ed., Boybeyi***
October, 1999

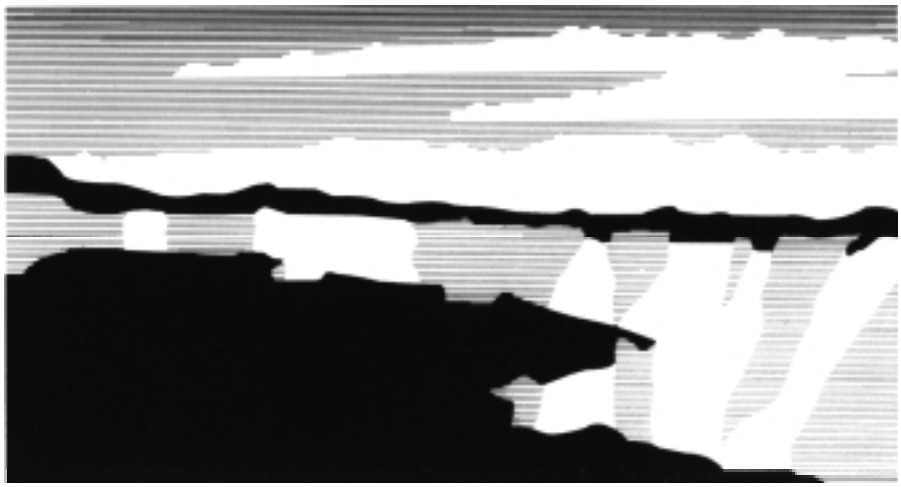

Los Alamos
NATIONAL LABORATORY

Form No. 836 R5
ST 2629 10/91

Urban parameterizations for mesoscale meteorological models

Michael J. Brown
Los Alamos National Laboratory
Energy and Environmental Analysis Group
Group TSA-4, MS F604
Los Alamos, NM 87545
E-mail: mbrown@lanl.gov

Abstract

Urban parameterizations developed for use in mesoscale meteorological models are described. These parameterizations attempt to account for the area-average effect of drag, turbulence production, heating, and surface energy budget modification induced by buildings and urban landuse. Some insights garnered through field observations regarding the urban influence on local meteorology are given, including short descriptions of the urban heat island and urban roughness. A brief survey of prior work on mesoscale modeling of urban areas is presented. Finally, problems that arise when implementing or validating the urban canopy parameterizations are discussed.

1. Introduction

Cities impact the local weather by perturbing the wind, temperature, moisture, turbulence, and surface energy budget fields. Buildings alter the wind, produce turbulent eddies, create shade, and trap heat. The urban fabric – made up of such materials as concrete, asphalt, and steel – stores and releases heat differently than rural areas. Energy consumption related to home and office heating and cooling, manufacturing, and transportation releases heat to the urban environment. Cities in arid environments may be wetter than their surroundings due to high water use, while cities in humid environments may be dryer due to replacement

of natural vegetation with urban materials. Urban-rural thermal differences can lead to generation of winds.

Numerous investigations have shown that buildings and urban landuse significantly modify the micro- and mesoscale flow fields (e.g., see reviews by Bornstein [1] and Hosker [2]). Accounting for the urban impact on atmospheric dynamics and thermodynamics is important for many applications, e.g., urban photochemical modeling, plume transport and dispersion, wind loading on buildings studies, urban design and energy usage studies, thermal comfort level evaluations, global warming assessments. For example, a plume trajectory may be modified by urban heat island circulations, the transport speed may be reduced due to building-induced drag, and vertical mixing might be enhanced as a result of heat island convection or building-created turbulence. For air quality applications and accidental release scenarios, mesoscale numerical models are often used to provide meteorological fields to air chemistry and puff dispersion models or boundary conditions to higher resolution models. Since mesoscale models do not have the spatial resolution to directly simulate the fluid dynamics and thermodynamics in and around urban structures, urban canopy parameterizations are sometimes used to approximate the drag, heating, radiation attenuation and enhanced turbulent mixing produced by the sub-grid scale urban elements.

In this chapter, we will focus on current methods for incorporating urban effects into mesoscale models. We will cover techniques for incorporating drag and turbulence production into the flow equations and modifications to the surface energy budget and heat equation to account for urban influences. We will distinguish between methods intended for use *above* the urban canopy from those intended to be used *within* the canopy. By necessity, we will present a short review of urban effects on mesoscale flows and will give references to more thorough reviews. We will end with a section on implementation and practical difficulties associated with the urban parameterizations, namely parameter specification and model validation issues. We will not cover the specifics of atmospheric dispersion in urban environments. We point the interested reader to very good reviews of urban impacts on dispersion by Hanna and Chang[3], Hanna et al.[4], Hosker[5], Yamartino et al.[6], and Brown and Streit[7].

2. Urban canopy impact on mesoscale flow

In the 1960's and 70's, the atmospheric sciences community began looking seriously at how cities impact the natural climate system (e.g., Chandler[8], Daigo and Nagao[9], Landsberg[10], Oke[11]). In the 1970's a number of groundbreaking urban field experiments were conducted, partially in response to air quality concerns in large metropolitan cities (e.g., Bornstein[12], Clarke[13], Ludwig[14], Oke and East[15], Angel et al.[16], Ackerman[17]). Likewise, in the late 60's and early 70's, computer models were first being used to understand the dynamics of urban-induced circulations and heating patterns (e.g., Myrup[18], Atwater[19], McElroy[20], Bornstein[21]). Based on these field experiments and numerical model results, the urban climate system was found to be multi-dimensional and complex with numerous feedback mechanisms between components. Explanations were hypothesized as to why many cities were warmer at night than the surrounding rural areas (coined the "urban heat island") and urban-scale flow patterns were found that were associated with these thermal differences. In addition, it became apparent that the drag and turbulence created by the "roughness" of buildings were large enough to reduce the strength of the mesoscale wind and enhance boundary-layer-scale mixing. In the next two sub-sections, we give short reviews of the so-called urban heat island and urban roughness effects. Our main purpose here is to identify the general flow features and mechanisms that are important to simulate and/or account for in mesoscale models. More complete accounts can be found in the excellent reviews by Oke[22] on the urban surface energy budget, by Bornstein[1] on urban circulation and thermodynamic evolution, and by Oke[23] on urban climate modification.

2.1 Urban heat island

The well-known urban heat island phenomenon is characterized by warmer temperatures in the city as compared to the surrounding rural area. Generally, the heat island occurs at night and results because the rural area cools faster than the urban area. Urban heat islands can induce thermodynamically driven urban-scale flows. In calm or low wind

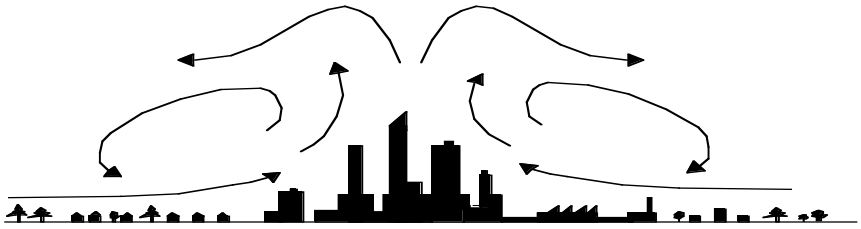

Figure 1. Illustration of urban heat island circulation during calm wind conditions. Pressure differences resulting from warmer temperatures in the city and cooler temperatures in the surrounding rural area lead to thermally-driven flows. Adapted from Lowry[24] and Liu et al.[25].

conditions, the warmer air in the city core rises, pulling air near the surface radially inwards (Fig. 1). A radially outward return flow may develop aloft. A dome of heated air often forms above the city. For slightly stronger ambient winds, a plume of heated air may extend downstream of the city.

Figure 2 shows temperature measurements at the surface for Okayama City, Japan and reveals the urban heat island signature. Temperatures are highest near the core of the city, where buildings are tall and urbanization is dense. Temperature differences of up to 10-12 K have been measured across large cities (Oke[23]). The vertical structure of the urban heat island often shows a several hundred meter well-mixed layer, as

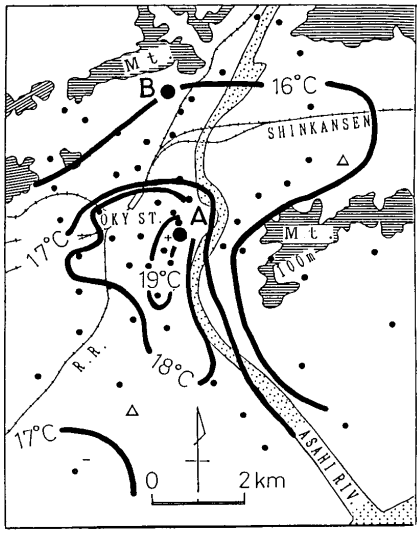

Figure 2. Surface temperatures observed at 21:00 local time for Okayama City, Japan. The hotter core is centered over the downtown area. From Sahashi et al.[26].

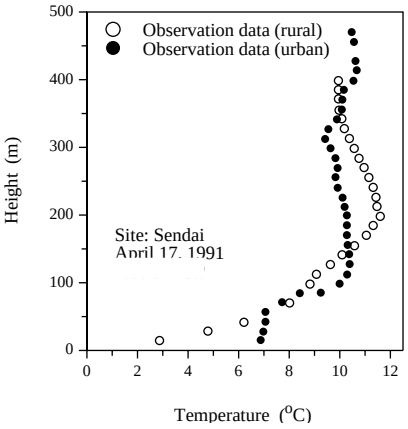

Figure 3. Nighttime temperature profiles at urban and rural sites reveal the heat island well-mixed layer. Adapted from Saitoh et al.[27].

indicated in Fig. 3. Here, a vertical profile of temperature outside of Sendai, Japan shows a deep stable layer, while the profile over the city reveals that the air temperature is uniform up to 50 meters and is warmer near the surface relative to the rural profile. Vertical profiles of the average of many urban-rural temperature difference measurements are given in Fig. 4 for the cities of New York, Christchurch, and Montreal. The profiles show a heated region extending from the surface to between 300 and 800 meters above the cities.

There have been fewer field measurements of the thermo-

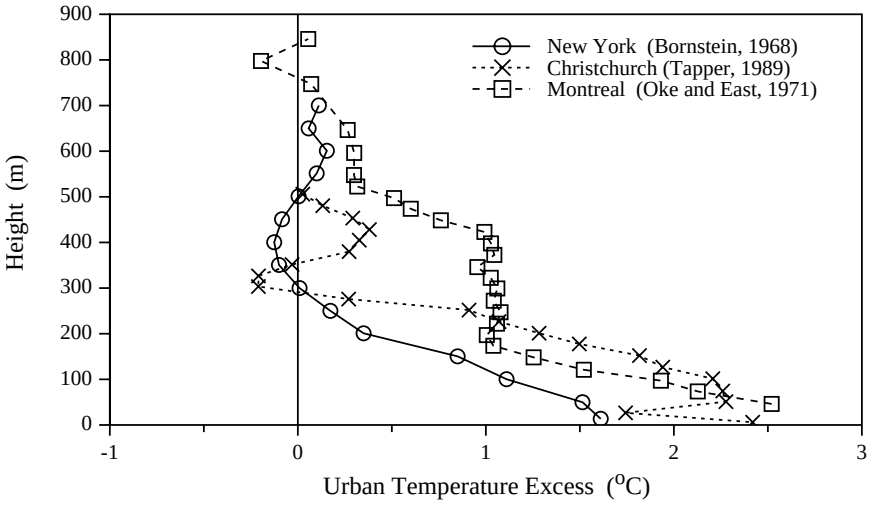

Figure 4. Average urban-rural temperature difference as function of height for 3 cities near sunrise. Adapted from Tapper[28].

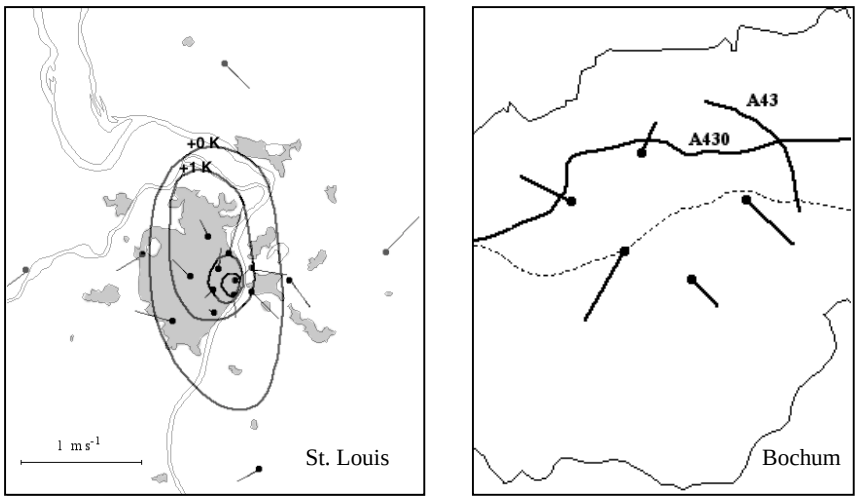

Figure 5. Urban heat island induced winds over St. Louis, USA and Bochum, Germany. Adapted from Shreffler[29] and Kuttler and Romberg[30].

dynamically-driven winds, in part because of the difficulty of separating the large and small scale components of the wind circulation. Climatological averages of surface wind sensor data in St. Louis, USA (Shreffler[29]) and Bochum, Germany (Kuttler and Romberg[30]) reveal radial inward motion (Fig. 5). These climatological averages were obtained during low wind speed conditions and in the former case by subtracting off the assumed prevailing wind components.

Although urban heat island intensity as measured by the maximum temperature difference between urban and rural sites correlates well with population, Oke's[31] review of existing measurements showed that European and North American cities collapsed onto two different curves (Fig. 6). Further analysis suggested that the difference was caused by the relatively taller buildings in the core of American cities. Figure 7 shows the urban heat island intensity plotted as a function of building height-to-width ratio, one measure of urban density. It should be pointed out that these data are for calm wind and cloudless conditions.

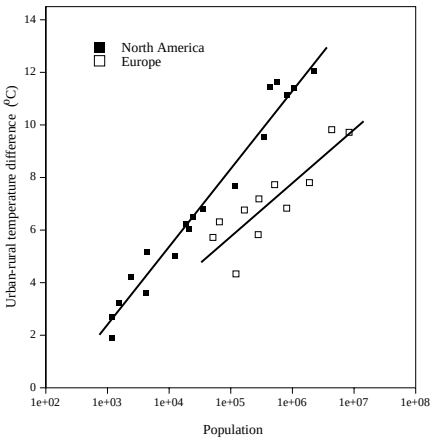

Figure 6. Measurements of urban heat island intensity as function of population showing differences in European and N. American cities (adapted from Oke[31]).

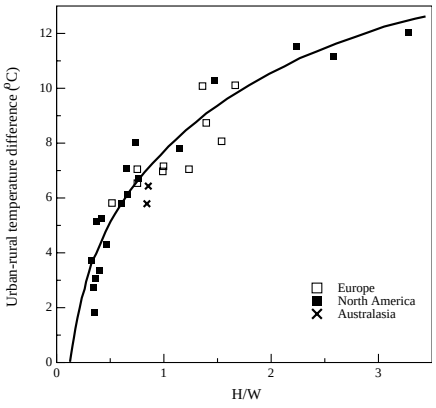

Figure 7. Measurements of urban heat island intensity as function of building height-to-width ratio (adapted from Oke[31]).

Although the measurements tend to collapse fairly well, results from numerous studies suggests that the formation and evolution of the urban heat island is complicated, dependent on a number of competing factors. For example, Fig. 8 indicates that the urban–rural temperature difference is a strong function of wind speed. If the winds are too strong, the heat can be advected away faster than it can be replenished by the city. In fact, Oke and Hannell[32] proposed that there is a critical wind speed above which urban heat islands do not form. They found that the critical wind speed U_c was a function of population P:

$$U_c = 3.4 \log P - 11.6 . \quad (1)$$

Relationships like those shown in Figs. 7 and 8 and eqn. (1) will be useful for direct testing and validation of mesoscale meteorological model results and indirect testing of the urban parameterizations.

Differences in the surface energy budget between urban and rural locales are suspected of being primary factors in the formation of the urban heat island. The energy balance in a

control volume containing the urban canopy can be written as (Oke[22])

$$\begin{aligned} Q^* + Q_F &= \left(R_{L\downarrow} - R_{L\uparrow}\right) + \left(R_{S\downarrow} - R_{S\uparrow}\right) + Q_F \\ &= \Delta R_L + (1-\alpha) R_{S\downarrow} + Q_F \\ &= Q_H + Q_E + \Delta Q_S + \Delta Q_A \end{aligned} \tag{2}$$

where Q* is the net radiation, Q_F is the anthropogenic heat flux, $R_{L\downarrow}$ and $R_{L\uparrow}$ are the downward and upward longwave radiation, respectively, $R_{S\downarrow}$ and $R_{S\uparrow}$ are the downward and upward shortwave radiation, respectively, ΔR_L is the net longwave radiation, $(1-\alpha)R_{S\downarrow}$ is the net shortwave radiation, α is the surface albedo, Q_H is the sensible heat flux, Q_E is the latent heat flux, ΔQ_S is the energy storage in the canopy, and ΔQ_A is the advection of energy into and out of the control volume. The net radiation represents the amount of energy coming into ($Q^* > 0$) or out of ($Q^* < 0$) the canopy from short and longwave sources. The energy associated with the net radiation and the anthropogenic heat flux is partitioned into the sensible heat flux (heats or cools the air), latent heat flux (evaporates water or condenses water vapor), energy storage (heats or cools urban surfaces), and advective heat flux (represents the energy transported by the wind into or out of the canopy volume). Later in Section 3.5 we will discuss eqn. (2) in more detail and present a slightly different form that we feel is more useful for mesoscale meteorological model implementation.

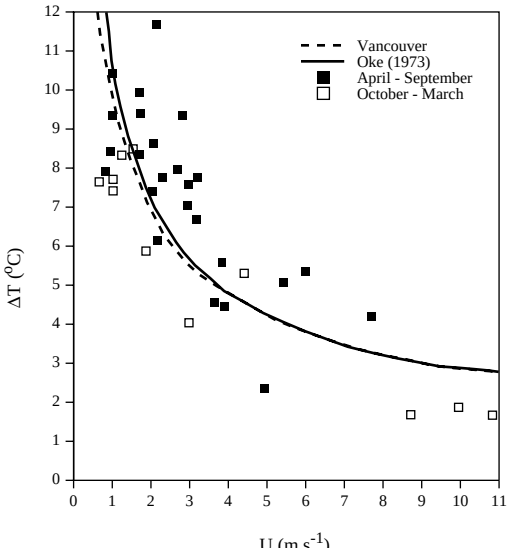

Figure 8. Measurements of heat island intensity plotted as a function of wind speed (adapted from Oke[33]).

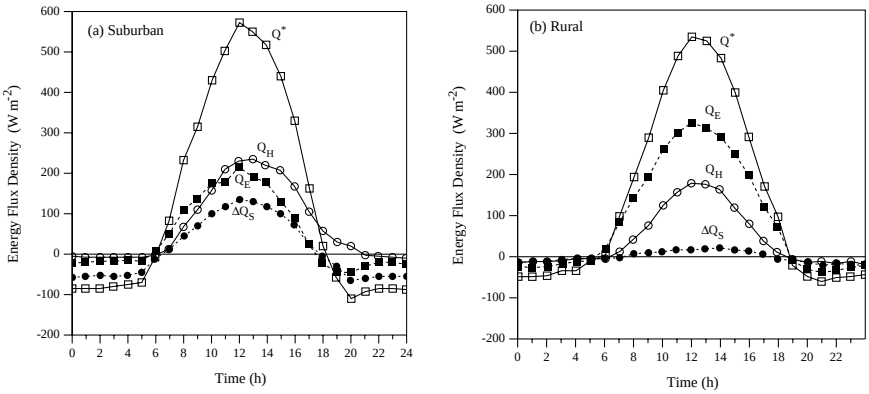

Figure 9. Surface energy balance measured over 30 days during the same time period at suburban and rural sites in Vancouver, BC (adapted from Oke[22]).

Figure 9 shows a diurnal cycle of surface energy fluxes for a suburban and a rural site in Vancouver. A number of major differences are apparent. First, the latent heat flux Q_E is much larger during the daytime at the rural site, indicating that the rural surface has more moisture than the suburban surface. Second, the canopy storage term ΔQ_S is much larger during the daytime at the suburban site, implying that the suburban canopy has more energy storage capacity. Third, the sensible heat flux Q_H remains positive for a few hours after sunset at the suburban site and the canopy storage term ΔQ_S reverses sign at night (i.e., the canopy mass gives off energy to the atmosphere) becoming relatively large in magnitude at the suburban site. This additional input of energy into the atmosphere helps to explain why the rate of cooling at night is smaller in the urban area and why temperatures would be warmer there. Additionally, the lack of a strong heat island during the daytime, which one might expect due to the small fraction of the net radiation Q* that goes into latent heating in the suburban area, is partially explained by the relatively large fraction of net radiation that goes into heating the canopy elements (ΔQ_S), thereby reducing the amount of energy that goes into heating the air (Q_H) in the suburban area.

Oke[22] lists seven (sometimes competing) causes for why cities may become warmer than the surrounding rural areas: 1) decreased longwave radiation loss due to reduced sky factor (i.e., the building walls trap, or

intercept, infrared radiation trying to escape up into the sky); 2) increased downward longwave radiation from the warmer air above the city (this may be due to trapping and re-emission from polluted layers aloft and/or from heat-island-induced vertical advection of warm surface air above the city); 3) increased shortwave absorption (the "bulk" albedo of urban areas is usually smaller than rural areas, possibly resulting from a combination of more surface area due to building walls and trapping of reflected solar radiation onto other urban surfaces due to canyon geometry); 4) decreased evapotranspiration due to less vegetation and moisture availability (this results in more energy going into heating the air and the canopy elements and less into latent heating of moisture); 5) anthropogenic heat input; 6) increased heat storage by canopy elements and 7) reduced heat transport (within the urban canopy the wind speeds and turbulent mixing are generally smaller).

Although decreased urban evapotranspiration, the anthropogenic heat flux, and the urban heat storage are major factors in the development of the urban heat island, it is difficult to draw general conclusions and the exact nature is site and time specific. For example, Oke[22] indicates that urban heat island development is a function of season (e.g., the anthropogenic heat flux increases in the winter for many northern latitude cities), the weather and local mesoscale flows (for example, seabreezes will interact with heat island development in coastal cities), local construction materials, local watering practices (for example, in downtown Mexico City it is common for the sidewalks to be cleaned every morning by hosing them down with water), and surrounding rural land use (e.g., rural areas surrounding arid southwestern U.S. cities will cool at a different rate than moist forest-covered midwestern and Atlantic seaboard cities).

Many of the factors cited above by Oke[22] are site and time dependent and have feedbacks with each other and with the flow field. Hence, it would be difficult to obtain universal functions for urban heat island intensity except for idealized cases. For modeling purposes, the individual factors need to be addressed in a robust way so that they interact reasonably. Several of the factors cited above are a strong function of the building height-to-width ratio (e.g., longwave radiation loss, shortwave absorption, wind speed, turbulent mixing) - which helps

to explain the strong dependence of urban heat island intensity on urban density (see Fig. 7). For broad application in different urban environments, a mesoscale meteorological model should have urban canopy parameterizations capable of capturing the effects of urban density as a function of landuse type, for example. In Sections 3.4 and 3.5, we present methods that have been used to approximate the effect of the urban canopy on heat transport and the surface energy budget in mesoscale models. Next we look at another manifestation of the city on the atmosphere: urban roughness.

2.2 Urban roughness

From the macroscopic viewpoint, cities can be thought of as rough surfaces. When flying high over a city and looking down, one can understand why buildings are often considered to be surface roughness elements. Mesocale models "see" the world similarly. With grid sizes on the order of kilometers, buildings are not resolved and hence are often parameterized as surface roughness.

Increased surface roughness, generally associated with urban areas, leads to greater frictional momentum loss and increased turbulent fluxes of heat, momentum, and moisture. The review by Bornstein[1] reports that several field studies show wind speed deficits generally exist in urban areas, while turbulence levels are generally elevated. For example, the climatological annual mean wind speed for an expanding city in Russia decreased over time from 3.9 m/s in 1945 to 2.6 m/s in 1971. An elegant study by Hogstrom et al.[34] illustrates the impact of the urban area on the vertical profile of wind speed (Fig. 10). By placing an instrumented tower at the urban-rural interface and doing conditional sampling based on wind direction, average wind speed profiles were obtained for both urban and rural fetch wind directions. It is expected that the reduction in wind speed by surface roughness will be offset somewhat by the speed up of the wind associated with the urban heat island circulation.

Surface measurements analyzed by Bowne and Ball[35] revealed that urban turbulence levels in Fort Wayne, Indiana were 30 to 50% higher than rural levels. Bornstein[1] found that surface measurements in and

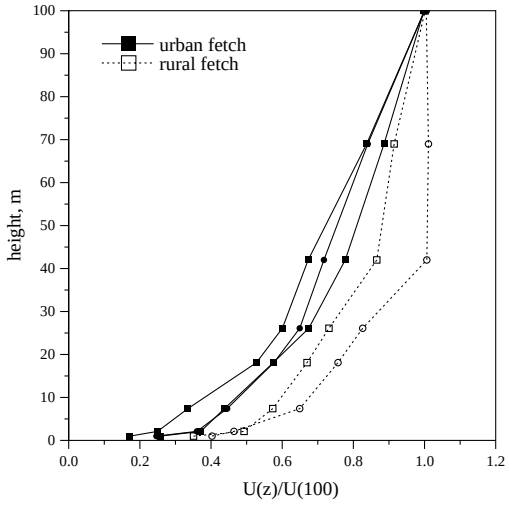

Figure 10. Average of many wind profiles measured on a tower during near-neutral conditions at an urban-rural interface (Hogstrom et al.[34]).

around New York City of the standard deviation of the horizontal wind direction σ_θ, a measure of turbulence intensity, indicated that values in the city were from 2 to 2.5 times greater than those in rural areas. Analysis of horizontal traverses over St. Louis by Godowitch[36] showed that the vertical velocity variance was about 50% larger as compared to outlying rural areas. It should be pointed out that these results include both the effects of urban heat island and roughness induced turbulence.

Wind-tunnel studies can isolate the surface roughness effect on wind and turbulence profiles. For example, Pendergrass and Arya[37] found that the mean velocity and Reynolds shear stress profiles for smooth surface and block roughness boundary layers were significantly different (Fig. 11). Theurer et al.[38] have performed a number of experiments over different configurations and shapes of building roughness elements. They found that wind speed and turbulence profiles above building rooftop are strongly impacted by the particular arrangement of buildings.

The studies cited above will be helpful in evaluating the wind and turbulence fields produced over cities. However, to understand the details of the parameterizations associated with urban roughness, it will be helpful to "zoom" down to the microscale and look explicitly at the flow fields around groups of buildings.

Numerous examples exist showing that wind flow patterns and turbulence mixing are dramatically altered around groups of buildings

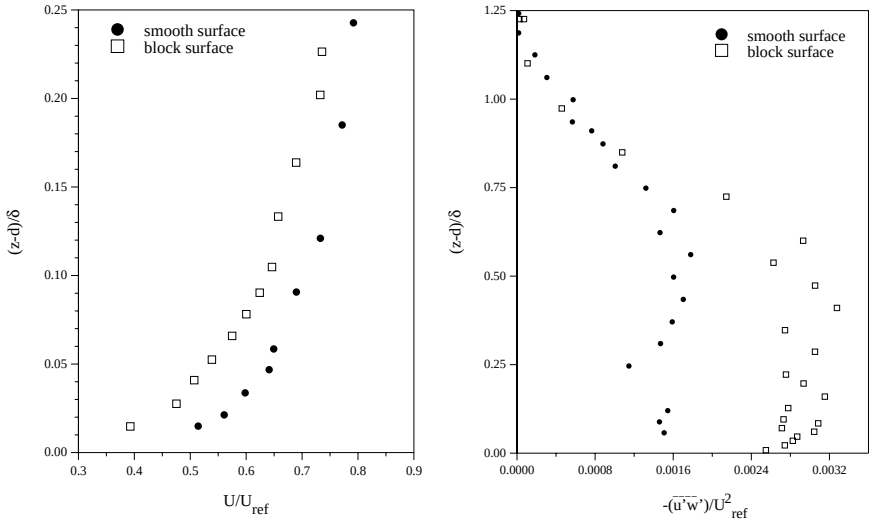

Figure 11. Comparison of non-dimensionalized mean wind profiles (left) and Reynolds shear stress profiles (right) for flow over a smooth surface and a block (urban) surface (Pendergrass and Arya[37]).

(e.g., Hosker[2]). Figure 12 depicts wind vectors and turbulence levels measured in a wind-tunnel around a rather simplified array of wide buildings. The measurements reveal vortices that form between the buildings in the street canyons, a jet region and recirculating flow above the first building rooftop, elevated turbulence levels above rooftop, and low turbulence levels in the street canyons. For rectangular buildings of equal height, the nature of the flow around the buildings is a function of the building width-to-height ratio. As summarized by Oke[22], a single vortex develops between buildings for skimming flow ($w/h < 1$), two counter-rotating vortices may develop for wake interference flow ($w/h \sim 1.5$), and for isolated roughness flow ($w/h > 3$) the flow field looks similar to the single building case (Fig. 13). Significantly more complicated flows can develop for groups of narrow buildings, for variable spacing between buildings, for buildings of different heights and shapes, and for different approach flow angles.

Few detailed mean and turbulence flow measurement campaigns have been performed within the real urban canopy. Roth[40] summarized

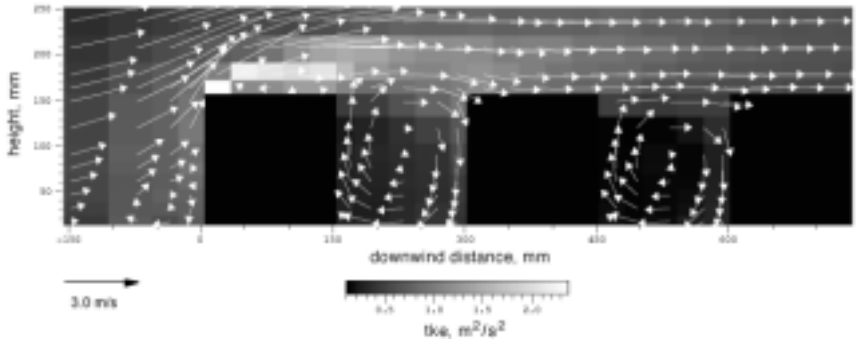

Figure 12. Wind vector and turbulent kinetic energy fields measured along centerline around a 2-d building array in the USEPA meteorological wind tunnel (Brown et al.[39]).

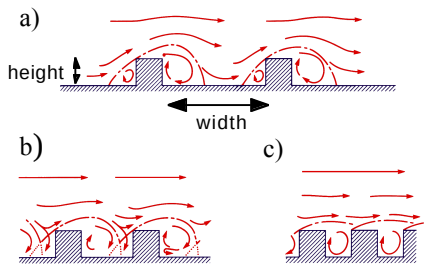

Figure 13. Flow regimes as function of width-to-height ratio: a) isolated roughness flow (w/h > 3); b) wake interference flow (w/h ~ 1.5); c) skimming flow (w/h < 1) (from Oke[22]).

results above the canopy layer in the so-called roughness sub-layer from 12 field experiments. He found that relationships derived from the logarithmic wind profile (see Section 3.2.2) described the data fairly well above the canopy height. Rotach[41] obtained a unique dataset containing vertical profiles of mean wind and turbulence statistics within and above an urban canopy in Zurich, Switzerland. Figure 14 shows mean wind and turbulent kinetic energy profiles averaged over many days of measurements. An inflection point is apparent in the mean wind profile, a signature of many vegetative canopy velocity profiles. Oikawa and Meng[42] measured mean wind and turbulence profiles in a suburban area in Sapporo, Japan that were in qualitative agreement with the

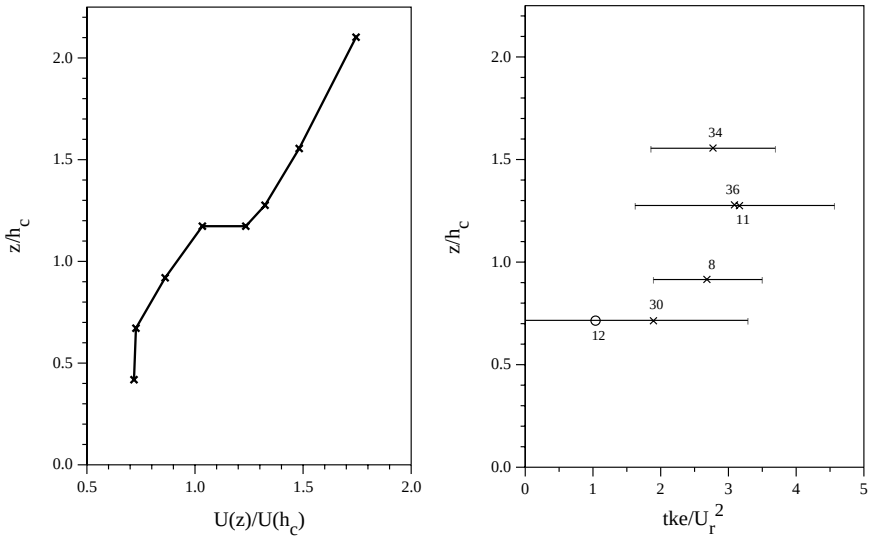

Figure 14. Average wind and turbulent kinetic energy profiles measured in a street canyon in Zurich (Rotach[41]). h_c is canopy height. Range and number of measurements are included on the tke plot.

measurements of Rotach[41]. They found that the Reynolds shear stress, a measure of the vertical turbulent momentum flux, peaked at about 1.5 times the canopy height.

As we have shown in this section, buildings act as a sink for momentum and result in a net loss of wind speed (see Section 3.2.1). The strong gradients in the wind produced by the buildings results in enhanced mechanical production of turbulence in the shear zones. The vertical variation of the area-average wind speed and tke is of course highly dependent on the arrangement, relative heights, and shapes of the buildings. For some applications, urban roughness parameterizations developed for mesoscale models should account for area-averaged drag and turbulent mixing effects and possibly be a function of the building geometry and configuration. In the next section, we discuss methods that have been developed for incorporating urban effects into mesoscale models.

3. Accounting for urban canopy effects in mesoscale models

In this section, we will describe several different methods for including urban canopy effects in mesoscale models. Although we will cover the more traditional methods (e.g., increasing the aerodynamic roughness length, altering the landuse properties), we will bias our discussion towards slightly more detailed approaches. However, we will not be focusing on microscale models in which the effects of buildings are explicitly accounted for, e.g., Arnfeld's[43] energy budget and radiation balance model, Murakami's[44] computational fluid dynamics models for flow around buildings. Rather we are looking at methods that attempt to parameterize the bulk, or area-average, effects of the urban canopy layer for use in mesoscale models. The "area-average" concept is a key one. We are not interested in simulating the details of what happens on particular street corners, but rather we want to compute the bulk effects of buildings and urban landuse over many square blocks, i.e., over a mesoscale grid cell which is typically on the order of kilometers in the horizontal dimension. In addition, we are assuming that the mesoscale model will have adequate resolution to resolve the canopy layer (if a model's first layer is hundreds of meters above ground level, then detailed urban canopy parameterizations would probably not be as beneficial).

Of course, the utility of the urban parameterizations will depend on the model and the model physics being used, so that some of the parameterization methods will not be applicable. For example, a diagnostic wind model may not be able to directly utilize the drag coefficient approach to account for the reduction in wind speed due to buildings. Or, a prognostic mesoscale code using empirical equations for the eddy diffusivity would most likely not be able to incorporate the turbulent kinetic energy production methods described below. Components of these parameterizations should be useful, however, for many of the operational and research mode mesoscale models that are in use today, e.g., COAMPS, FITNAH, HOTMAC, MEMO, MERCURE, MM5, OMEGA, RAMS. Below, we will discuss methods for incorporating urban effects into the momentum, turbulent transport, heat, and surface energy budget equations. First we give a brief overview of

past research work where urban parameterizations have been incorporated into mesoscale and boundary-layer models.

3.1 Summary of urban parameterization modeling efforts

Myrup[18] was one of the first to numerically model the details of the urban energy budget. Surface energy balance equations similar to (2) were solved numerically, while atmospheric conditions were prescribed (i.e., prognostic equations for the atmospheric flow field were not solved). Urban values of the roughness length z_0, the ground albedo α, the soil heat capacity C_p, the soil conductivity k_s, and relative humidity were required to specify the surface energy fluxes. Using this simple model, Myrup[18] was able to simulate reasonable urban-rural temperature differences and found that reduced evaporation and increased roughness in cities, the thermal properties of urban materials, and the wind speed were major factors in determining the strength of the heat island. Without prognostic equations for the atmospheric dynamics, however, he was not able to look at the feedback mechanisms between the flow field and the surface energy budget. More recent work (e.g., Oke et al.[46], Mills [47]) has incorporated urban canyon influences on the urban energy budget, including shadowing, multiple long- and shortwave reflections off walls and ground surfaces, and heat flux from building interiors. Oke et al.[46] found that the building spacing (width-to-height ratio) and the thermal properties of the urban canopy were controlling variables for urban heat island intensity.

Delage and Taylor[47], Bornstein[21] and Vukovich et al.[48] numerically simulated the urban heat island circulation using the atmospheric conservation equations for mass, momentum, and heat. They did not solve a surface energy budget equation, but rather defined different surface temperatures or cooling rates for the urban and rural areas in the modeling domain. Urban effects were captured through the roughness length z_0 and the specified urban-rural temperature differences. Model simulations were found to reproduce many of the characteristics of the urban heat island circulation. For example, in the 2-d simulations performed by Bornstein[21], a critical upstream wind speed was found that resulted in either faster or slower winds over the urban area, a result of the dual competing effects of urban roughness-induced drag and

thermally-induced winds. In 3-d simulations, Vukovich et al.[48] found cyclonic inflow around the heat island for low wind speeds. They found that as the ambient wind speed increased, the urban heat island intensity decreased and the length of the downwind thermal plume increased. Although much was learned about the development of urban heat island circulation, they were not able to study the feedback mechanisms between different components of the energy balance and the flow field.

Some of the first simulations performed using linked atmospheric flow and surface energy budget equations were performed by Atwater[19] and McElroy[20]. Although the simulations were 2-d, steady-state in the case of McElroy[20], and included no advection in the case of Atwater[19], they were able to look at how the surface energy budget modified the wind fields, how the modified wind fields changed the surface energy budget terms, and so forth. In both cases, anthropogenic heat flux terms were added to the surface energy budget and urban-specific ground albedo, roughness length, thermal diffusivity, density, and heat capacity were defined. The effect of urban-induced drag and mixing were accounted for through the roughness length parameter. McElroy[20] found reasonable agreement between the model-computed thermal structure in the boundary layer and experimental measurements. Atwater[19] also included the effects of radiatively-active pollutants in the surface energy budget and introduced a moisture availability term for computing the latent energy flux term. Although the pollution layer was shown to reduce incoming solar radiation, Atwater[19] found that the physical properties of the surface were more important in the creation of the urban heat island .

2-d and full 3-d mesoscale atmospheric simulations utilizing surface energy budget equations and the roughness length approach have been performed over urban areas by a number of modelers, e.g., Hjelmfelt[49], Schultz and Warner[50], Byun and Arya[51], Kimura and Takahashi[52], Saitoh et al[27], Mochida et al.[53], Carissimo[54], Kitada et al.[55], Hafner and Kidder[56], Taha[57], Perez-Garcia and Nickerson[58]. They have performed simulations in St. Louis, Los Angeles, El Paso, Tokyo, Paris, Nagoya, Atlanta, and Mexico City with reasonable success. Using a larger roughness length to account for the urban influence on drag and eddy diffusivity and incorporating the anthropogenic heat flux into the surface energy budget, several of the investigators were able to simulate

qualitatively reasonable looking urban heat islands. As will be discussed below in Section 3.2, these simulations did not capture the flow dynamics within the urban canopy. In addition, they did not account for the effects of radiation attenuation, trapping, and emission due to buildings.

Sorbjan and Uliasz[59] were among the first to incorporate urban-canopy induced drag and turbulence production directly into the fluid dynamics equations (as opposed to the roughness length approach which is incorporated through boundary conditions). They introduced a drag term into the horizontal momentum equations and a turbulent generation term into the eddy diffusivity profile formula. Using this approach they were able to compute the flow fields *within* the urban canopy. Also unique to their study was the introduction of a turbulent generation term associated with vehicles and the adaptation of Atwater's[19] radiation scheme to account for pollution on the development of the urban heat island.

Based on forest canopy parameterizations of Yamada[60], Williams et al.[61] included urban-induced drag and turbulent production terms into a mesoscale model with a q^2-l turbulence closure. Like Sorbjan and Uliasz[59], they included a drag term in the horizontal momentum equations, but also included a turbulence production term in the turbulent kinetic energy ($q^2/2$) equation. In addition, as outlined in Brown and Williams[62], the radiation attenuation due to the urban canopy was crudely accounted for in the surface energy budget while the heat flux from rooftops and vertically-distributed anthropogenic heat sources were included in the heat conservation equation.

Recently, a number of researchers have developed similar urban canopy parameterizations with different levels of complexity for k-ε turbulence closure models. Maruyama[63], Urano et al.[64], and Ca et al.[65] have all included the urban canopy drag term in the momentum equations. Maruyama[63] included urban-induced drag terms in the turbulent kinetic energy (k) and the turbulent dissipation rate (ε) equations as well. The surface energy balance was ignored however. Urano et al.[64] included drag and turbulence production terms in their k-ε mesoscale model and solved an energy balance equation at the ground surface. Like Brown and Williams[62], they added a vertically-varying anthropogenic heat flux term to the heat equation as well. Ca et al.[65] did not add urban production terms to the turbulent kinetic energy or

dissipation terms, but like Maruyama[63] did include an effective air volume term in the mass, momentum, heat, turbulent kinetic energy, and dissipation equations. The effective air volume term accounts for the reduced air volume in the grid cells within the urban canopy. Ca et al.[65] included a detailed radiation balance model accounting for shading and multiple reflections of long and shortwave radiation off of building walls and streets in their surface energy budget model. They also included a building air conditioning model to explicitly account for heat emissions and feedback between urban temperature and air conditioning usage.

3.2 Drag

The drag force induced by buildings and other obstacles in the urban environment results in a transfer of momentum out of the bulk flow and a reduction in the area-average wind speed (see Section 2.2). A number of different methods have been used in mesoscale and boundary-layer modeling in order to account for the drag effect. In this section, we will look at three methods that cover a range of complexity: the popular roughness length approach in which the wind profile is modified in the lowest grid cell through boundary conditions; a straightforward attenuation approach in which the wind profile is modified through the canopy layer using empirically-derived formulae; and a drag formulation which gets incorporated into the prognostic momentum equations. First we begin with a definition and derivation of the drag term.

3.2.1 Drag force definition

The drag force is the force that a fluid exerts on a solid (e.g., Whitaker[66]). The solid may be the earth's surface, buildings, trees, a car, an airplane, among other things. The drag force on an object is in the same direction as the mean flow (in addition, there may also be a lift force that develops off-angle to the mean flow depending upon the geometry of the obstacle). The drag is typically divided into form, or pressure, drag and frictional, or viscous, drag. Form drag is a result of the pressure differential that forms around objects when enveloped in a flow field (usually the front face of an obstacle has a high pressure associated with the flow impacting the front surface and the back face has

a low pressure that is a function of whether or not flow separation occurs on the back side). The frictional drag is a result of mixing of momentum in a direction normal to the surface of the object. The fluid elements closest to the object "stick" to the surface, shear layers develop, and either molecular or turbulent diffusion transports the slow moving fluid away from the obstacle resulting in momentum loss around and downstream of the solid object.

By definition, the drag force F_D on an obstacle is the integral of the pressure and viscous forces over the surface of the obstacle (e.g., Panton[67]):

$$F_{D_x} = \int n_x P - n_i \tau_{ix} dS, \tag{3}$$

where x is the direction of the flow, n_x is the unit normal vector parallel to the flow, P is the pressure (or perturbation pressure), n_i is the unit normal vector perpendicular to the surface, and τ_{ix} is the shear stress term. For laminar flows, τ_{ix} represents molecular viscous forces while for turbulent flows it includes the turbulent Reynolds shear stresses.

As a body force, the drag force term can be added to the right hand side of the atmospheric fluid flow momentum conservation equation:

$$\rho \frac{DU_i}{Dt} = -\frac{\partial P}{\partial x_i} - \rho g \delta_{i3} - 2\rho \Omega \varepsilon_{ijk} \eta_j U_k + \frac{\partial \tau_{ji}}{\partial x_j} - \frac{\rho F_{D_i}}{\delta V}, \tag{4}$$

where ρ is the fluid density, U_i is the mean velocity in the i^{th} direction, $D(\ )/Dt = \partial(\ )/\partial t + U_j \partial(\ )/\partial x_j$ is the total derivative, P is the pressure, g is the gravitational acceleration term, δ_{i3} the Kronecker delta function, Ω is the angular velocity of the earth's rotation, ε_{ijk} is the permutation tensor, η_j is the unit vector parallel to the earth's axis of rotation, τ_{ij} the shear stress tensor, and δV a unit volume. F_{Di} is defined to be positive in the direction opposite to the mean flow U_i. For incompressible flows, the shear stress tensor τ_{ij} can be written out in turbulent and viscous components, i.e.,

$$\tau_{ij} = -\rho < u_i u_j > + \mu \frac{\partial U_i}{\partial x_j}, \tag{5}$$

where u_i is the pertubation from the mean velocity, the < >'s represent an ensemble average, $\langle u_i u_j \rangle$ is the Reynolds turbulent shear stress term, and μ is the molecular viscosity.

The non-dimensionalized form of the drag force, called the drag coefficient C_D, is obtained by dividing the drag force by the mean kinetic energy of the flow and the cross-sectional area of the obstacle:

$$C_D = \frac{F_D}{\frac{1}{2}\rho U_0^{\,2} A}. \tag{6}$$

For idealized flow conditions and obstacle shapes, analytical solutions for C_D can be obtained (e.g., Panton[67]). For more realistic flow conditions and obstacle shapes, C_D is determined experimentally (e.g., Hoerner[68]). Assuming one knows C_D for a given obstacle and flow condition, the drag force imparted by the obstacle on the flow can be computed with additional knowledge of only a reference velocity U_0 and the cross-sectional area of the obstacle A.

3.2.2 Aerodynamic roughness length approach

Drag due to the urban surface is commonly accounted for in mesoscale models by modifying the surface roughness parameter associated with the lower boundary conditions of the model. Many mesoscale codes using Monin-Obukhov similarity relationships for defining the turbulent fluxes and/or the mean flow variables at the lowest grid cell above the surface. One of the parameters in the Monin-Obukhov similarity relationships is the aerodynamic roughness parameter z_0 which influences the gradients of the flow variables and the magnitude of turbulent mixing at the surface.

Monin-Obukhov similarity states that the wind shear in the surface layer is a function of a velocity scale and two length scales (e.g., Arya[69]), i.e.,

$$\frac{\partial U}{\partial z} = \frac{u_*}{\kappa z}\phi_m(z/L), \tag{7}$$

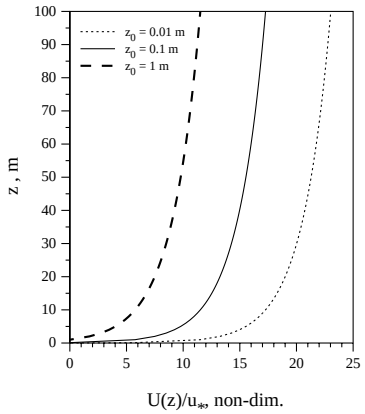

Figure 15. Logarithmic velocity profile for neutral conditions as function of z_0.

where U is the mean wind velocity in the direction of the wind, z is the height above ground, u_* is the friction velocity ($u_*^2 = \langle uw \rangle_0$), u and w are the horizontal and vertical velocity pertubations, respectively, k is von Karman's constant (0.4), ϕ_m is a stability-dependent, empirically-determined function that relates the turbulent shear stress to the mean velocity gradient, and L is the Obukhov length that pertains to the relative importance of shear and buoyancy effects in the surface layer.

Integrating eqn. (7) from U=0 to U=U(z) and assuming the turbulent momentum flux is constant within the surface layer, one obtains the logarithmic velocity profile:

$$U(z) = \frac{u_*}{\kappa}\left[\ln\frac{z}{z_0} - \psi_m(z/L)\right], \tag{8a}$$

where z_0 is the roughness length and ψ_m are stability-dependent corrections to the mean velocity profile. The roughness parameter z_0 can be thought of as the height above the surface at which U goes to zero. Figure 15 shows how the mean velocity profile changes with z_0 given a constant u_* and neutral conditions.

For very rough surfaces, such as urban and forested areas, a displacement height d is needed for the logarithmic profile method to work. That is, the surface reference plane should be moved up off the ground to some fraction of the roughness element height h:

$$U(z) = \frac{u_*}{\kappa}\left[\ln\frac{z-d}{z_0} - \psi_m\left(\frac{z-d}{L}\right)\right]. \tag{8b}$$

Arya[69] showed how z_0 relates to the drag coefficient by equating the surface stress τ_0 to the mean wind speed at a reference height z_r through a drag relation:

$$\tau_0 = \rho C_D U(z_r)^2 \tag{9}$$

Assuming neutral stability, substituting u_*^2 for τ_0/ρ and eqn. (8) for $U(z_r)$, and rearranging, Arya[69] obtained:

$$C_D = \frac{\kappa^2}{\left\{\ln[(z_r - d)/z_0]\right\}^2} \tag{10}$$

Hence, as the roughness length increases, the frictional drag increases as well (fig. 16).

In practice, the roughness length is incorporated into mesoscale simulations in one of two ways. In many mesoscale codes the velocity at the first grid level above the surface is specified as a boundary condition using the logarithmic velocity profile eqn. (8). In this approach, the effect of surface roughness is transmitted directly through the boundary condition to the velocity field. Alternatively, some codes prognostically compute the velocity at the first grid level using the momentum conservation equations and use eqn. (7) as a boundary condition to specify the wind shear in the Reynolds shear stress computation at the lowest grid cell. The roughness length z_0 is used to compute u_*. using eqn. (8), which is then used to determine the wind shear boundary condition. In a similar way, the roughness length also influences the boundary condition computations of the heat and moisture fluxes, which are derived from Monin-Obukhov similarity as well (see Section 3.5).

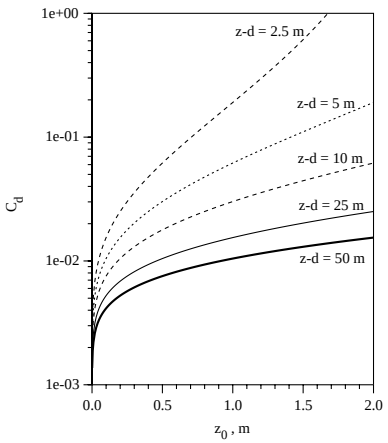

Figure 16. Variation of drag coefficient C_D with roughness length z_0 at different heights according to eqn. (10).

The advantage of the aerodynamic roughness approach is that it is easy to

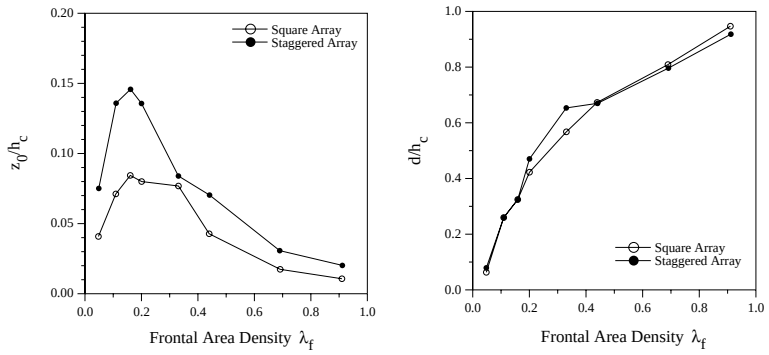

Figure 17. Wind-tunnel measurements of roughness length and displacement height as function of frontal area density for cubes in square and staggered arrays (adapted from Hall et al.[71]).

implement and considerable information is available for specifying z_0 and d as a function of landuse type. Simple formulae have been developed that relate z_0 and d to the canopy element height h_c (e.g., Plate[70]):

$$z_0 = 0.15\ h_c \quad \text{and} \tag{10a}$$

$$d = h_c\ . \tag{10b}$$

In reality, z_0 and d are functions of canopy element (e.g., building, tree, bush) spacing, shape, stiffness, relative heights, etc. For example, wind-tunnel experiments by Hall et al.[71] show that closely spaced buildings have a larger displacement height than widely spaced buildings and the roughness length initially increases as the building density increases and then decreases beyond a critical density (Fig. 17). Early work by Letau[72] provided a relationship for z_0 that considered the frontal area density λ_f:

$$z_0 = 0.5\ h_c\ A_f/A_d = 0.5\ h_c\ \lambda_f\ , \tag{11}$$

where A_f is the total frontal area of the obstacles and A_d is the total area covered by the obstacles. This expression was found to be valid for small λ_f (< 20 to 30 percent), i.e., for sparsely populated building arrays.

Raupach[73], Bottema[74], McDonald et al.[75], and Duijm[76] derived relationships for z_0 and d incorporating the sheltering effect of building obstacles which are valid over a wider range of λ_f. For example, McDonald et al.[75] proposed the following:

$$z_0 = \frac{h_c - d}{h_c} \exp\left[-\frac{0.5 C_D \lambda_f}{k^2} (1 - \frac{d}{h_c}) \right] \text{ and} \tag{12a}$$

$$d = h_c \cdot \left\{ 1 + A^{-\lambda_p} (\lambda_p - 1) \right\}, \tag{12b}$$

where λ_p is the plan area density (plan view area of obstacles divided by total plan area) and A is a constant that depends on obstacle arrangement. McDonald et al.[75] found that A=4.4 and 3.6 worked well for staggered and aligned arrays of square blocks, respectively. Although it is not clear which formulae are "best", we direct the reader to careful evaluations that have been carried out by Grimmond and Oke[77] and Duijm[75].

There are a number of disadvantages to the aerodynamic roughness approach which might be problematic depending on the application. First, the lowest height at which winds can be computed with the logarithmic formula is at the displacement height d (typically a large fraction of the urban canopy height). This provides problems when one is interested in what happens at street level (e.g., street-level dispersion, surface heat fluxes). So, in fact, when a modeler presents results of winds at the lowest level using a roughness length approach as described above, these winds are actually at or above the building rooftops. A second disadvantage is that the horizontally-homogeneous condition used in the Monin-Obukhov similarity theory is not satisfied within and for some distance above the urban canopy. Plate[70] reported that field experiments above vegetative canopies showed that the logarithmic profile was valid for $z > 2h_c$. For an urban canopy, Roth[40] found that above $2.5h_c$ Monin-Obukhov similarity appeared to work well. Lastly, traditional Monin-Obukhov similarity cannot account for the inflection point in the velocity profile (nor the elevated peak in tke) as was shown in Fig. 14. The methods described in the next two sections attempt to overcome these limitations.

3.2.3 Attenuation approach

Much work has been done accounting for drag within the vegetative canopy layer. Numerous mean wind profiles have been measured in the within real and artificial plant canopies such as corn, wheat, orchards, forests, wooden pegs, and plastic strips (e.g., see Cionco[78], Plate[70], Arya[69]). Early work by Cionco[78] included the following formula for flow within the canopy:

$$U(z) = U(h_c)\exp\left[b(z)\cdot\left(\frac{z}{h_c}-1\right)\right], \tag{13a}$$

where U(z) is an area-average wind velocity, $U(h_c)$ is the wind velocity at canopy height, and b(z) is an attenuation coefficient dependent on the plant canopy. In Fig. 18, eqn. (13a) is plotted for several values of b and yields the expected sharp decay with height in the canopy, but does not approach zero at the surface. As presented in Pielke[79], a slightly different formulation has been proposed that does go to zero at the surface:

$$U(z) = U(D)\exp\left[b\cdot\left(\frac{\ln z}{\ln D}-1\right)\right]. \tag{13b}$$

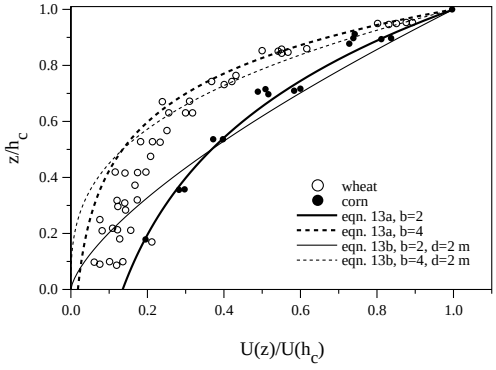

Figure 18. Comparison of eqns. (13a) and (13b) to measurements made in vegetative canopies (after Arya[69]).

Eqn. (13b) is also plotted in Fig. 18 assuming that $D=h_c$. Note that this formulation does not work for D less than or equal to one.

As described in Cionco and Ellefsen[79], these attenuation methods can be extended to urban canopies. Eqn. (13) could be used as a boundary condition in place of the logarithmic velocity profile (eqn. (8)) or could be used to extrapolate below the

lowest grid level in coarse vertical resolution simulations. In addition, this approach could be easily adapted for use with diagnostic wind models (whereas the drag approach we describe below in the next section would be more difficult to implement). The method is straightforward, but does require specification of the attenuation coefficient which is a function of the canopy type and also may be a function of height.

The functional form of b(z) can be derived for several idealized cases. Following the derivation presented in Arya[69], for steady-state, horizontally-averaged flow within a canopy, the conservation equation for momentum (eqn. (4)) reduces to:

$$\frac{\partial < uw >}{\partial z} = -\frac{1}{\rho}\frac{\partial P}{\partial x} - \frac{1}{2} C_D a(z) U^2 \tag{14}$$

where a(z) is the effective aerodynamic canopy surface area per unit volume of canopy ($A/\delta V$). If one assumes that the horizontal pressure gradient is negligible (perhaps valid near the top or above the canopy), then eqn. (14) reduces to a balance between the gradient of the turbulent shear stress and the drag force. Using the mixing length hypothesis to describe the Reynolds shear stress, i.e.,

$$< uw >= -l_m^{\,2} \left(\partial U / \partial z\right)^2, \tag{15}$$

and assuming that $C_d a(z)$ and the mixing length l_m are constant, eqn. (14) can be integrated to yield eqn. (13a) with

$$b = h_c \cdot \left(\frac{C_d a}{4 l_m^{\,2}} \right)^{1/3}. \tag{16}$$

Although attenuation coefficients have been experimentally-determined for a number of plant canopies (e.g., Cionco[78]), we are unaware of b(z) values for urban canopies. In addition, the assumptions that were used to simplify eqn. (14), namely that the pressure gradient is negligible, is not valid within the urban canopy where form drag is dominant. However, the form of eqns. (13a-b) may still describe the horizontally-averaged urban canopy velocity profile adequately for many model applications.

3.2.4 Drag approach

As shown in Section 3.2.1, a drag force term can be added to the atmospheric momentum conservation equations to account for obstacle drag. This approach has been successfully used to parameterize the frictional drag due to forest canopies (e.g., Wilson and Shaw[81], Yamada[60], Liu et al.[82]) and has been used in several cases for urban canopies (e.g., Sorbjan and Uliasz[59], Brown and Williams[62], Urano et al.[64]). Using the drag coefficient approach, modifications can be made to the horizontal components of the momentum equations to account for the area-average effect of the sub-grid urban canopy elements:

$$\frac{DU}{Dt} = -\frac{1}{\rho}\frac{\partial P}{\partial x} + fV - \frac{\partial < uu_j >}{\partial x_j} - f_{urb} C_d a(z) U|U|, \tag{17a}$$

$$\frac{DV}{Dt} = -\frac{1}{\rho}\frac{\partial P}{\partial y} - fU - \frac{\partial < vu_j >}{\partial x_j} - f_{urb} C_d a(z) V|V|, \tag{17b}$$

where f is the Coriolis parameter, the $<u_i u_j>$ are the Reynolds shear stresses, f_{urb} is the fraction of the grid cell covered by urban canopy, a(z) is the canopy area density (surface area of buildings perpendicular to the wind per unit volume of urban canopy), and the other variables are as defined in eqn. (4). The drag force will be non-zero within the canopy and "turn-off" at some height above the canopy in response to the canopy area density a(z) term. The drag formulation by Urano et al.[64] and Sorbjan and Uliasz[59] is nearly identical to eqn. (17), except in the latter case they lumped C_d and a(z) together and did not explicitly state that it could vary with height.

In these approaches, it is assumed that the sub-grid buildings affect the flow field, but do not take up any volume within the grid cell. Maruyama[63] and Ca et al.[65] included a fractional volume term G in the conservation equations to account for the space occupied by buildings. If one assumes that the building canopy actually occupies volume within the computational domain, then this approach ensures that mass fluxes are conserved across grid cells. In principle, even without the drag terms added, the flow will slow down or speed up as it travels

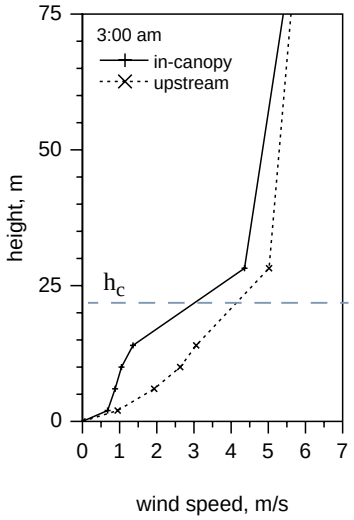

Figure 19. Model-computed wind speed profile at non-urban (upstream) and urban (in-canopy) sites (Brown and Williams[62]). Canopy height = 22 m.

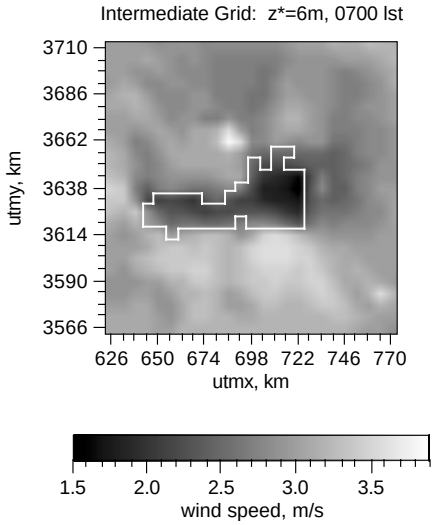

Figure 20. Mesoscale simulation of Dallas/Ft. Worth area (white outline) showing wind speed reduction over the urban area due to drag parameterizations (Brown and Muller [86]).

through grid cells with more or less air volume. It is not clear what the relative impact of the G and drag terms are on simulations. Some authors (e.g., Hirt[83]) have used the fractional volume approach to account for the drag effect of sub-grid forest canopies and assumed that the G term accounted for the drag, i.e., no drag force term was needed. Porous flow approaches are somewhat similar to the drag approach as well, adding a frictional term to the equations that is similar in behavior to the C_d term (e.g, Ingram et al.[84]). Bottema and Sini[85] found that traditional porous flow methods did not work well for urban simulations, basically because the frictional force was too small, i.e., porous flow dynamics did not well represent the flow within an urban canopy.

This drag method has the advantage over the roughness length approach in that the effects of the canopy can be applied to the flow interior, not just as a boundary condition. As shown in Fig. 19, the model

can account for the height variation of the wind profile within the canopy. Figure 20 shows the impact on the mesocale flow field. The simulation, performed over Dallas, illustrates the wind speed reduction over the urban area due to the drag force. The major disadvantage with the drag approach includes specifying the new terms that need to be incorporated into the model, including the drag coefficient C_d, the canopy area density a(z), and the urban grid cell fraction f_{urb}. We discuss their specification in Section 4.1.

3.3 Turbulence Production/Destruction

Buildings result in enhanced turbulence production in the urban environment. The flow blockage, isolated regions of jetting, and adverse pressure gradients associated with the building obstacle result in flow separation, recirculation zones, high shear, and production of turbulent eddies. Within the street canyon, turbulent mixing may be suppressed due to a disconnection with the ambient airflow above. In this section, we will look at three methods that have been used in mesoscale modeling for incorporating enhanced turbulent mixing due to building obstacles: the roughness length approach; a local scaling method; and a drag formulation. All three methods either directly or indirectly modify the Reynolds shear stress term, often modeled as a first-order gradient diffusion term:

$$< u_i u_j >= -K_m \left(\frac{\partial U_i}{\partial x_j} + \frac{\partial U_j}{\partial x_i} \right), \tag{18}$$

where K_m is the turbulent eddy diffusivity for momentum.

3.3.1 Roughness length approach

As discussed in Section 3.2, the roughness length influences the friction velocity (i.e., the surface layer turbulent momentum flux) through the surface boundary conditions. For urban surfaces, the larger roughness length results in a larger friction velocity u_* through eqn. (8). Depending on the turbulent closure scheme and the particulars of the boundary condition formulation, the eddy diffusivity, the Reynolds shear stress, and/or the velocity gradient at the lowest vertical grid level are enhanced

due to their dependence on the friction velocity. In this way, the surface roughness associated with urban landuse affects turbulent mixing.

Although this approach is easy to implement, it is valid only at some height above the canopy where the flow is quasi-horizontally homogeneous. As mentioned in Section 3.2.2, Roth[40] found that Monin-Obukhov similarity appeared to work well over an urban area above $2.5h_c$. Using the roughness length approach, one cannot account for the expected peak in turbulent mixing at or above the canopy height and the reduced mixing within the street canyons. The approach has worked well, however, for defining the general characteristics of the urban heat island.

3.3.2 Empirical local scaling approach

Similar to the approach proposed by Cionco[78] for accounting for canopy drag on the wind profile (Section 3.2.2), an equation describing the vertical profile for turbulent kinetic energy, eddy diffusivity, or Reynolds shear stress could be formulated within and/or above the urban canopy. Based on an extensive review of field data, Roth[40] proposed the following formulae for a locally-scaled friction velocity u_* and the turbulence intensity in the roughness sublayer above the urban canopy:

$$\begin{aligned} \left(-<uw(z)>\right)^{1/2} &= u_*(z) \\ &= U\cdot\left\{0.095+0.389\exp\left[-0.971\cdot(z-d)/h_c\right]\right\} \end{aligned} \tag{19a}$$

and $$I_i = \sigma_i / U = \kappa A_i \left[\ln\left(\frac{z-d}{z_0}\right)\right]^{-1}, \quad i = u, v, w, \tag{19b}$$

where σ_u, σ_v, and σ_w are the standard deviations of the horizontal and vertical components of the wind velocity components and A_i is an empirical constant (Fig. 21). Rotach[87] proposed an alternative expression for the friction velocity within the roughness sublayer:

$$u_*(z) = u_*\cdot C_1\cdot\left\{1-\exp\left[-C_2\cdot(z-d)\right]\right\}^{1/3}, \tag{20}$$

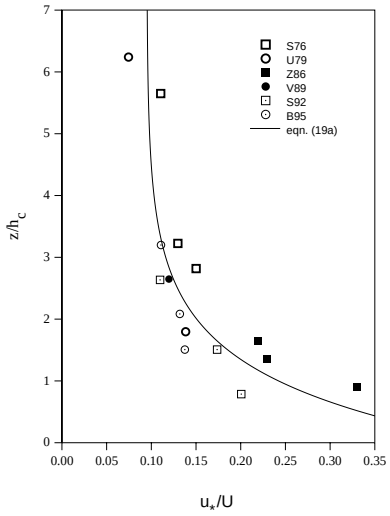

Figure 21. Eqn. (19a) compared to measurements of the friction velocity over urban areas (Roth[40]).

where u_* is the friction velocity above the roughness sublayer within the inertial sublayer and C_1 and C_2 are experimentally-determined constants. Rotach[87] proposed equations for the velocity variances that were non-dimensionalized by the local friction velocity eqn. (20). In both cases, the equations can be used to extrapolate down to the canopy element height using wind velocities or friction velocities computed by the mesoscale model at the top of the roughness sublayer. These methods could be used to provide finer details within the first grid cell for vertically-coarse resolution mesoscale simulations or to complement diagnostic wind models by providing turbulence parameters for dispersion modeling applications. We are not aware of any area-average formulations for the turbulent kinetic energy, eddy diffusivity, or Reynolds shear stress *below* canopy height.

3.3.3 Drag approach

In mesoscale models using the k-ε or q^2-*l* turbulence closure approach to specify the eddy diffusivity, a turbulent kinetic energy production term can be added to the tke equation to account for urban-induced turbulence, (e.g., Brown and Williams[62], Maryuma[63], Urano et al.[64])

$$\frac{Dtke}{Dt} = \delta_{i3}\frac{g}{\Theta} < u_i\theta > - < u_i u_j > \frac{\partial U_i}{\partial x_j} - \frac{\partial < u_j \cdot tke >}{\partial x_j} - \frac{1}{\rho}\frac{\partial < u_i p >}{\partial x_i} - \varepsilon + f_{urb} C_d a(z)\left(|U|^3 + |V|^3\right). \quad (21)$$

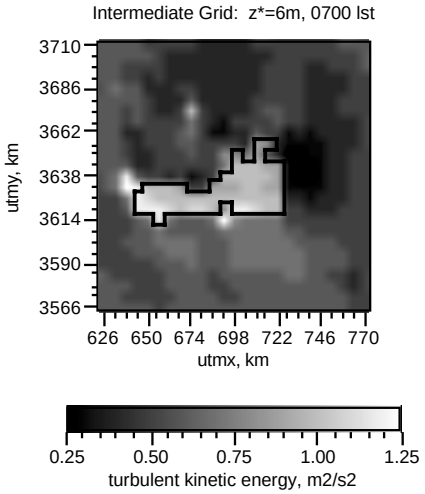

Figure 22. Model-computed tke over the Dallas/Ft. Worth area (black outline) showing high tke values over the urban area (Brown and Muller[86]).

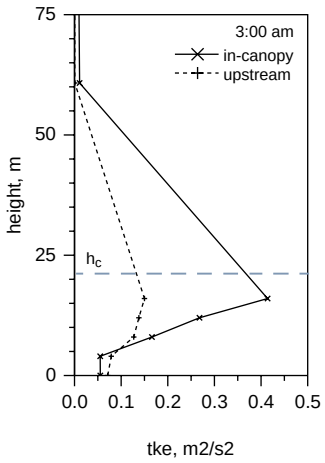

Figure 23. Comparison of tke profiles computed within and upstream of urban canopy (Brown and Williams[62]).

where tke = k = $q^2/2$ = 1/2($<u^2>+<v^2>+<w^2>$) and ε is the dissipation term. This is the exact form of the tke equation without the closure assumptions used in k-ε or q^2-*l* modeling applied yet. The last term is the tke production term due to sub-grid urban canopy elements, where f_{urb} is the urban fraction of the grid cell, C_d is a drag coefficient, a(z) is the canopy area density, and U and V are the horizontal components of the wind velocity. The absolute value signs on the velocities insure that the drag term is always a source of turbulent kinetic energy. Little justification has been given for the form of the tke production term, except that it is dimensionally correct. Figures 22 and 23 show the impact of the drag term on tke levels in a mesoscale simulation over an urban area.

Similarly, drag terms have been added to the modeled dissipation equation (e.g., Maryuma[63])

$$\frac{D\varepsilon}{Dt} = \frac{c_{\varepsilon 1} P_k}{\rho}\frac{\varepsilon}{tke} - c_{\varepsilon 2}\frac{\varepsilon^2}{tke} + \frac{\partial}{\partial x_j}\left(\frac{K_m}{\sigma_\varepsilon}\frac{\partial \varepsilon}{\partial x_j}\right), \\ + f_{urb} C_d a(z)\frac{\varepsilon}{tke}\left(|U|^3 + |V|^3\right) \tag{22}$$

and the modeled q^2-l equation (e.g., Yamada[60])

$$\frac{Dtke \cdot l}{Dt} = \frac{\partial}{\partial z}\left[\frac{tke^{1/2} \cdot l \cdot \tilde{S}_q}{2}\frac{\partial tke \cdot l}{\partial z}\right] + \frac{l \cdot E_1}{2}\left[< u_i u_j > \frac{\partial U_i}{\partial x_j} + \beta g < w\theta >\right], \\ -\frac{tke^{3/2}}{2B_1}\left[1 + E_2\left(\frac{l}{kz}\right)^2\right] + f_{urb} \cdot C_d \cdot a(z) \cdot l \cdot \left(|U|^3 + |V|^3\right) \tag{23}$$

where $c_{\varepsilon 1}$, $c_{\varepsilon 2}$, σ_e, E_1, E_2, and B_1 are empirically-determined coefficients and S_q is a stability-dependent factor. Note that the dissipation eqn. (22) does not have a buoyancy term included.

Eqns. (21) and (22) are similar to those proposed by forest canopy modelers (e.g., Wilson and Shaw[81])). Liu et al.[82] proposed adding a sink term to eqns. (21) and (22) to account for the accelerated cascade of tke to small scales due to small-size leaf foliage. It is not clear whether a sink term is needed for urban canopies. Ayotte et al.[88] incorporated drag terms into a 2nd order turbulence closure model for vegetative canopy flow. From this type of modeling, one might be able to learn how to better parameterize the first-order closure models described above.

For mesoscale models using empirical formulae for determination of the eddy diffusivity, K_m can be modified as a function of height using the drag approach to account for building obstacle effects. Based on an approximated solution to a simplified form of the turbulent kinetic energy equation, Sorbjan and Uliasz[59] obtained the following formula for the eddy diffusivity within the urban canopy for neutral conditions:

$$K_m = l^2\left\{\left|\frac{dU}{dz} + \frac{dV}{dz}\right|^3 + \frac{E_c}{l^2}\right\}^{1/3}, \tag{24}$$

where E_c is the rate of urban-generated turbulent kinetic energy defined by

$$E_c = 1/2 \cdot C_d \cdot a(z) \cdot \left(U^2 + V^2\right)^{3/2}. \quad (25)$$

This formulation results in a larger eddy diffusivity above urban surfaces with precise values determined by the specification of the drag coefficient C_d and the canopy area density a(z). Sorbjan and Uliasz[59] did not modify *l* within the urban canopy.

3.4 Heat equation

In this section, two possible modifications to account for urban effects in the atmospheric conservation equation for heat are discussed. The first is radiative heating or cooling aloft due to pollution associated with urban activities. The second is related to ambiguities in how to define the urban surface and whether it is best to account for urban canopy heating terms in the surface energy budget or in the atmospheric heat conservation equation.

3.4.1 Heating aloft associated with urban pollution

Clearly, urban haze and smoke can impact the transference of short and longwave energy through the atmosphere and thus impact the surface radiation budget. In addition, pollutant layers above the city can absorb energy resulting in warming of the air aloft and can emit energy resulting in local cooling. The modification of the thermal structure could lead to changes in the heat island circulation and intensity.

In a 2-d numerical modeling study, Atwater[19] found that carbonaceous aerosols resulted in a small amount of warming (0 to 0.5 K) aloft over urban areas during the daytime. Interestingly, however, he found that over rural areas a 0.5-1.0 K heating aloft occurred due to absorption of solar radiation. The increased stability reduced the growth of the mixed layer over the rural area by one-half. The small amount of heating over the urban area did not impact the mixed-layer growth and Atwater[19] hypothesized that this was because the heat flux associated with the pollutant layers was negligible compared to the anthropogenic and other urban heat flux terms. Using a more sophisticated Mie-

scattering radiation scheme, Yoshida and Kunitomo[89] found 0.5 – 1.5 K daytime heating aloft in a 1-d simulation of the atmosphere. The amount of warming was determined to be a function of aerosol diameter.

3.4.2 Urban canopy heating terms

The Reynolds-averaged form of the conservation equation for heat is given by

$$\frac{D\Theta_V}{Dt} = -\frac{\partial}{\partial x_j} < u_j \theta_V > + \frac{1}{\rho C_p} \frac{\partial R_N}{\partial z} \ , \tag{26}$$

where Θ_v is mean virtual potential temperature, $<u_j\theta_v>$ is the turbulent heat flux, ρ is the density of air, C_p the specific heat capacity of air, and R_N is the net radiation ($R_{S\downarrow} - R_{S\uparrow} + R_{L\downarrow} - R_{L\uparrow}$). The last term represents the flux divergence of net radiation and can be either a source or sink of heat.

For a mesoscale model with adequate vertical resolution to resolve the urban canopy layer, but with horizontal grid spacing on the order of kilometers, it becomes somewhat ambiguous on where to define the surface and how to spatially attribute heat sources due to buildings and urban activities. Rather than add the anthropogenic heating term to the surface energy budget equation, Ca et al.[65], Urano et al.[64], Brown and Williams[62], and Taha[57] assumed that the heat is released directly to the air. In addition, Brown and Williams[62] assumed that the rooftop heat flux was emitted directly to the air. As shown in Fig. 24, the model grid cell can be divided into an urban fraction (f_{urb}) and non-urban fraction ($1-f_{urb}$), and then the urban canopy fraction can be further subdivided into roof fraction (f_{roof}) and "between-building" fraction (f_{cnyn}). A modified heat equation is then obtained:

$$\begin{aligned} \frac{D\Theta_V}{Dt} = & -\frac{\partial}{\partial x_j} < u_j \theta_V > + \frac{\left(1 - f_{urb}\right)}{\rho C_p} \frac{\partial R_N}{\partial z} + \\ & \left(1 + \frac{1}{B}\right)^{-1} \left(\frac{f_{cnyn}}{\rho C_p} \frac{\partial R_{N_c}}{\partial z} + \frac{f_{roof}}{\rho C_p} \frac{q_{roof}}{\Delta z} \right) + \frac{f_{urb} q_{urb}}{\rho C_p \Delta z} \end{aligned} \tag{27}$$

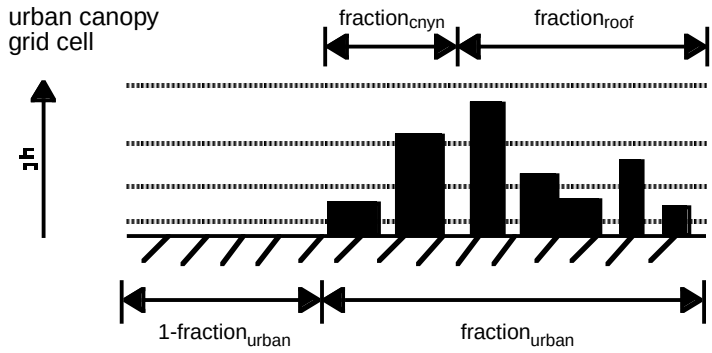

Figure 24. Illustration of how each urban grid cell is divided up into urban and non-urban fractions. The urban fraction is further sub-divided into roof and canyon fractions (Brown and Williams[62]).

where R_{Nc} is the net radiation within the canopy, B is the Bowen ratio (sensible to latent heat flux ratio), $(1+1/B)^{-1}$ is the fraction of energy that goes into heating the air, q_{roof} is the amount of energy emanating from the rooftop, and q_{urb} is the anthropogenic heat flux in a particular height interval. In most prior atmospheric modeling studies, the roof and anthropogenic heating terms have been accounted for in the surface energy budget equation, not in the heat equation.

Urano et al.[64] included a height-varying anthropogenic heat flux in the heat equation, however, they sub-divided the anthropogenic heat flux into the heat and surface energy budget equations. They split the anthropogenic heat flux from vehicles equally between the heat and surface energy budget equations, and allocated all the anthropogenic heat flux from the 1st floor of buildings to the surface energy budget equation and above the 1st floor to the heat equation. They found that the vertical distribution of heat significantly impacted surface temperatures in their model simulations of the Tokyo urban heat island. In principal, the anthropogenic heat flux could be multiplied by the $(1+1/B)^{-1}$ term, however, in most studies it has been assumed that all the anthropogenic energy goes into heating the air.

Brown and Williams[62] calculated the rooftop heat flux from

$$q_{roof} = R_{N_{hc}} - R_{L_{roof}} = (1-\alpha_{roof})R_{S\downarrow} + \Delta R_{L_{hc}} - \varepsilon_{roof}\sigma T_{roof}^{\ 4} \ , \qquad (28)$$

where α_{roof} is the rooftop albedo, ε_{roof} is the rooftop emissivity, and T_{roof} is the rooftop temperature. Implied in eqn. (28) is the assumption that the rooftop is infinitely thin and all solar radiation absorbed by the roof is immediately reemitted as longwave and sensible heat, i.e., the roof has no heat storage capacity. Without further information, they assumed that the rooftop longwave radiated at air temperature, clearly an underestimation during the daytime. For a better approximation, one could solve a "surface" energy budget equation at rooftop and solve for the rooftop temperature T_{roof}. In addition, inclusion of the heat flux from building walls into eqn. (23) or at a minimum accounting for their extra surface area in the surface energy budget equation might be important as well (e.g., Voogt and Oke[90]).

The net radiation within the canopy is assumed to exponentially decay as the ground is approached:

$$R_{N_C}(z) = R_{N_{hc}} \exp[-k \cdot bai(z)] \ , \qquad (29)$$

where R_{Nhc} is the net radiation at canopy top, k is an extinction coefficient, and bai(z) is the cumulative "building" area index (analogous to the leaf area index) defined as

$$bai(z) = \int_z^{h_c} a(z')dz' \ , \qquad (30)$$

where a(z) is the canopy area density (note that the canopy area density for drag, e.g., eqn. (17), is the surface area of the buildings perpendicular to the mean wind per unit volume, while here the surface area is the plan area of the buildings per unit volume). The extinction coefficient k should be a function of time of day as the sun angle changes. The net radiation approach described here is a modification of the forest canopy parameterizations proposed by Yamada[60]. For that reason, it is considered to only be a crude approximation for the net radiation attenuation within the urban canopy. Methods based on sky-view factor or derived from explicit radiation balance modeling around clusters of

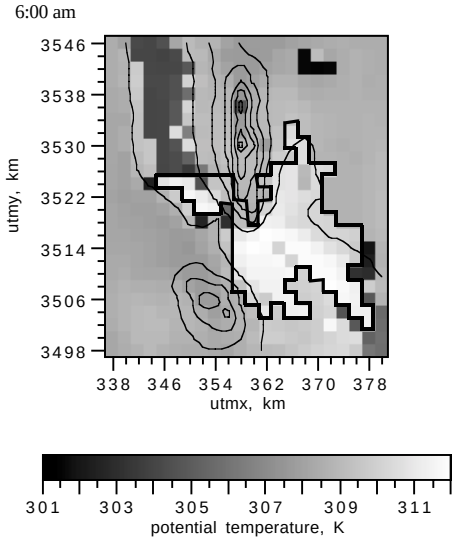

Figure 25. Near-surface temperatures computed over the El Paso/Ciudad Juarez region showing urban heat island (Brown and Williams[91]). Urban area denoted by black outline.

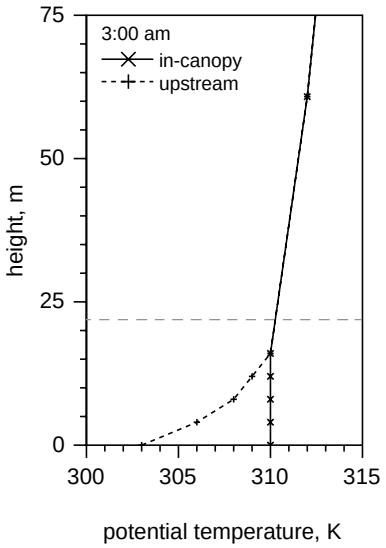

Figure 26. Comparison of model-computed profiles of potential temperature within and upstream of the urban canopy (Brown and Williams[62]).

buildings should be considered in order to improve the radiation attenuation formulation (e.g., Oke et al.[45], Mills[46], Ca et al.[65]).

Figure 25 shows near-surface temperatures over the El Paso/Ciudad Juarez region from a simulation that utilizes the urban heating parameterizations described above. A several degree urban heat island intensity is apparent. Figure 26 shows the vertical potential temperature profile of an idealized urban heat island simulation. The profile shows a well-mixed region within the canopy.

3.5 Surface energy balance

The surface energy balance is solved in order to define the surface temperature, a boundary condition for the mesoscale model. Typically, the surface energy budget is defined at the ground plane by making a

balance equation for the amount of incoming and outgoing energy. For urban areas, it is difficult to specify exactly where the ground is located: is it at street level running under the buildings, a surface that follows the contours of the building surfaces, a horizontal plane that is defined at rooftop? In principal, separate energy balance equations could be solved at rooftop, on building sidewalls, and at street level as in the microscale models of Arnfeld[43], Mills[46] and Ca et al[65]. This is not practical for typical mesoscale modeling applications, as the level of detail needed to define the building layout for an entire city is typically not readily available (if one could define "typical" building configurations for different types of urban landuse (e.g., downtown, high density residential, low density residential, commercial, residential) and/or as a function of height-to-width ratios or canopy area density, then this approach might be more practical for mesoscale applications).

Eqn. (2) has been used by many mesoscale modelers for defining the surface energy budget over urban areas, with and without the canopy storage and anthropogenic heat flux terms. This method places a control volume around the canopy elements, computes the heat fluxes at the top and sides of the box, and assumes that there is a canopy heat storage term within the volume. A simple, straightforward approach for accounting for the urban impact on the surface energy budget eqn. (2) has been outlined by Taha[57] and Perez-Garcia and Nickerson[58]. They incorporated the objective hysteresis model of Grimmond et al.[92]. This model defines the urban canopy storage term ΔQ_S in eqn. (2) as a function of the net radiation Q* based on experimental measurements:

$$\Delta Q_S = \sum_{i=1}^{n} \left(a_i Q^* + b_i \frac{\partial Q^*}{\partial t} + c_i \right) A_i \,, \tag{31}$$

where a, b, and c are empirical coefficients associated with landuse, n is total number of landuse types, and A_i is the area fraction of the particular landuse within the area of interest (e.g., model grid cell). Taha[57] incorporated the anthropogenic heat flux term into the lowest grid cell of the heat equation, however, and added a soil heat flux term Q_G in the surface energy budget and scaled it by the non-urban grid cell fraction ($1-f_{urb}$).

However, although this method of enclosing the urban canopy elements within a control volume is conceptually appealing and useful for understanding the partitioning of the energy budget, it is not particularly amenable to mesoscale model applications where one wants to solve for the meteorological fields *within* the urban canopy. In Brown and Williams[62], the surface energy budget equation is defined at ground-level and is slightly different than that given by eqn. (2):

$$\begin{aligned} Q^* &= (R_{L\downarrow} - R_{L\uparrow}) + (R_{S\downarrow} - R_{S\uparrow}) \\ &= (1-f_{urb})\{(1-\alpha_G)R_{S\downarrow} + \Delta R_L\} + f_{cnyn} R_{N_{h_c}} \exp[-k \cdot bai(0)] \\ &= Q_H + Q_E + Q_G \end{aligned} \qquad (32)$$

where α_G is the ground albedo in the non-urban area, and ΔR_L is the net longwave radiation, R_{Nhc} is the net radiation at canopy height, k is an extinction coefficient, and bai(z=0) is the cumulative building area index as defined in eqn. (30). As discussed in Section 3.4, the model grid cell was divided into urban and non-urban fractions, and then the urban fraction was subdivided into canyon and rooftop fractions. The first term on the right hand side on the second line represents the net longwave and net shortwave radiation in the non-urban fraction of the grid cell, while the last term represents the fraction of the solar and longwave radiation that reaches ground-level in the urban canyon fraction of the grid cell. Following the forest canopy work of Yamada[60], it is assumed that the grid-cell averaged net radiation falls off exponentially in the urban canopy. The solar radiation that is intercepted by the rooftops is assumed to be converted to heat and then directly emitted into the air through the heat eqn. (27), therefore the rooftop fraction of the solar radiation is not put into the surface energy budget eqn. (32).

As in many of the modeling studies cited in Section 2, the advective term ΔQ_A was omitted from surface energy budget eqn. (32) because the mesoscale model explicitly accounts for heat advection. In addition, the anthropogenic heat flux Q_f was put into the heat eqn. (27) rather than in the surface energy budget eqn. (32). The reasoning for this was that the anthropogenic heat flux is emitted into the air (e.g., heat loss from buildings, vehicle-related heat emissions) and its distribution with height could be better accounted for in the heat conservation equation. The

anthropogenic flux term will still impact the surface energy budget, but indirectly through heating of the air aloft and changing the magnitude of the flux terms, most notably the sensible heat flux Q_H.

The soil or ground heat flux can be approximated by

$$Q_G = K_s \left. \frac{\partial T_s}{\partial z_s} \right|_G , \tag{33}$$

where K_s is the soil diffusivity and the soil temperature gradient at the ground can be obtained solving a one dimensional heat conduction equation in the ground. K_s is typically modified to account for the diffusivity properties of urban materials. One might also consider variation with depth in the urban materials, for example, a street would have an asphalt layer overlying a road bed of packed soil or a wall might have an outer plaster layer and then wood, insulation, and/or dead air space underneath.

Here we wish to clarify that Q_G is the energy flux into and out of ground and urban surfaces (asphalt, concrete, masonry, etc.), while Q_f is the energy flux from human activities, primarily the heat released from energy use. So Q_f includes heated air escaping from buildings to the atmosphere, while Q_G also includes energy fluxes from the building surfaces, but just that component associated with the heat received from the atmosphere (in the form of short and longwave radiation). In practice, it may be difficult to distinguish between the two fluxes when measured experimentally. In addition, it might be prudent to subtract off the roof fraction from the soil flux term in eqn. (32), so that only the ground heat flux occurs for the non-urban and street canyon ground surfaces. However, as pointed out by Voogt and Oke[90], the extra surface area associated with the non-anthropogenic heat flux into and out of building walls should be considered in the heat balance eqn. (32). Hence, the overestimation of the surface area in the first case and the underestimation in the second case may offset one another.

As an alternative to solving the heat conduction equation, the simpler force-restore method can be used to compute the surface temperature (e.g., Kimura and Takahashi[53], Carissimo[54]):

$$\frac{\partial \Theta_G}{\partial t} = \frac{2\omega}{k \cdot C_p}(\Delta R_S + \Delta R_L - Q_H - Q_E) - \omega(\Theta_G - \Theta_D), \qquad (34)$$

where Θ_G is the ground surface temperature, $\omega = 2\pi/24$, k is soil heat conductivity, C_p is soil heat capacity, and Θ_D is the deep soil temperature.

The final terms in eqn. (32) that need to be evaluated are the sensible and latent heat fluxes

$$Q_H = -\rho C_p u_* \Theta_* \quad \text{and} \qquad (35a)$$

$$Q_E = -\rho L_v u_* q_*. \qquad (35b)$$

They are typically evaluated using Monin-Obukhov similarity relationships to define the friction velocity u_*, the temperature scale Θ_*, and the water vapor scale q_* , i.e., eqn. (8) and

$$\Theta(z) - \Theta_G = \frac{\Theta_*}{\kappa}\left\{\ln\left(z/z_{o_t}\right) - \Psi_h(z/L)\right\}, \qquad (36a)$$

$$Q_W(z) - Q_{W_G} = \frac{q_*}{\kappa}\left\{\ln\left(z/z_{o_v}\right) - \Psi_v(z/L)\right\}, \qquad (36b)$$

where L_v is the latent heat of vaporization, Θ_G and Q_{WG} are ground level temperature and mixing ratio of water vapor, respectively, Pr and Sc are the turbulent Prandtl and Schmidt numbers, respectively, z_{0t} and z_{0v} are the roughness lengths for temperature and water vapor, respectively, and Ψ_h and Ψ_v are stability correction functions. The heat balance eqn. (32) can be used iteratively with eqn. (36a) to solve for the ground-level temperature Θ_G.

Determination of the latent heat flux is problematic since its magnitude depends on Q_{WG}, which depends on the underlying moisture content of the surface. Oke[23] gives equations for the surface water balance, but since the moisture content of urban areas is a function of recent weather, watering practices, and urban cover, it is very difficult to simulate the water balance. Often rather simplifying assumptions are used to specify the latent heat flux. For example, Brown and

Williams[62] and Ca et al.[65] specify a Bowen ratio for the urban canopy, so that the latent heat flux is calculated directly from the sensible heat flux:

$$Q_L = Q_H / B. \tag{37}$$

Mochida et al.[53], Kimura and Takahashi[52], and Atwater[19] utilized similar moisture availability equations to compute Q_{Wg}. Mochida et al.'s[53] version is

$$Q_{wg} = q_g = q(z) + \beta(q_{sat} - q(z)), \tag{38}$$

where β, the moisture availability constant, is specified for different landuse types and varies from 0 for dry surfaces to 1 for water bodies and q_{sat} is the saturation water vapor mixing ratio at the surface temperature. Basically eqn. (38) says that the ground can act as a source of moisture (q_{sat}) and that the flux of moisture is proportional to the difference between the amount of moisture in the ground and the amount in the air (q_{sat}-q(z)). In general, β is small for urban landuse and larger for vegetated and moisture laden landuse.

An important item to note is that Monin-Obukhov similarity is being used to specify boundary conditions at the surface *within* the urban canopy. As discussed earlier, Monin-Obukhov similarity falls apart in the canopy layer. However, without alternative "theories" there is no other recourse as the surface boundary conditions must be specified in order to run the numerical model. Research on alternative approximations for how to specify area-averaged surface fluxes within the canopy layer would be extremely valuable.

4. Practical difficulties

4.1 Parameter specification

The drawback of potentially more universal, in-depth urban parameterizations is that there is often a corresponding need to specify

more or new parameters. A major challenge lies in determining the different coefficients that are needed for the urban canopy parameterizations. Data is often sparse and may contain large uncertainties. As outlined in Sections 3.2 and 3.3, the advantage of using the urban roughness approach to account for some of the effects of the urban canopy is that there are numerous references on the roughness length z_0 and displacement height d for urban areas. However, there still is quite a bit of uncertainty in the specification of even these parameters (e.g., Grimmond and Oke[77]) and the method cannot account for many of the within-canopy effects of buildings. In this section, we give typical ranges for some of the parameters needed to implement the urban canopy drag, heating, and surface energy budget parameterizations as given in eqns. (17), (21), (27) and (32).

Landuse. Urban landuse needs to be specified as a function of space within the mesoscale modeling domain. In the approach of Brown and Williams[62], the fraction of the horizontal grid cell area occupied by urban landuse f_{urb} needs to be defined. In the approach of Ca et al.[65] and Maruyama[63] the fractional volume occupied by buildings needs to be determined for each grid cell. The area fractions can be evaluated from landuse datasets which are often freely available online (e.g., the USGS Landuse/Land Cover dataset). These datasets, however, can be outdated and there is often ambiguity in determining the urban fraction based on the given landuse categories. Determination of the building volume fractions would require specialized datasets or some mapping of typical landuse categories into volume fractions.

Many of the urban parameters are a function of the urban landuse type or building density and therefore it may be useful to break down urban landuse into finer sub-divisions. Brown and Williams[62] have divided the urban landuse into four classes: downtown/city center, industrial/commercial, residential with mature trees, and residential w/out mature trees. The principal distinguishing characteristics between these categories are built vs. green space fractions, canopy height, and building density. The canopy height is utilized in defining the depth through which the urban canopy impacts the flow field through such parameters as the canopy area density a(z). In addition, the surface energy budget and heat conservation equation parameterizations given by eqns. (27) and

(32) require specifying the building rooftop and street canyon fraction of the grid cell area. Although these quantities are site-dependent, Table 1 provides typical ranges found in the literature.

Surface Properties. A number of landuse-dependent surface properties are needed for the urban surface energy balance eqn. (32). For example, an extinction coefficient or sky view factor should be utilized in determining the net radiation attenuation within the urban canopy. Specification of the Bowen ratio or moisture availability coefficient is especially problematic as their value depends on weather and city watering policy, but generally a larger Bowen ratio and a smaller moisture availability coefficient is expected as the urban fraction increases. Residential areas, in general, should have more moisture availability than downtown, industrial, or commercial areas. A range of measured values is given in Table 1. One could try to model the urban water balance, but this is often beyond the realm of atmospheric mesoscale modeling.

Urban and rooftop albedo and emissivity measurements cover a wide range of values as well and generally have not been broken down by urban landuse type. However, albedos specific to different types of building rooftops have been published in the literature (e.g., Oke[23]). There can be some ambiguity in what measured albedos represent, i.e., do the measurements include the effect of building wall reflections (a sort of area-average urban albedo) or is it representative of a particular surface (such as an asphalt road or a tile roof)? It is often stated that the albedo of urban areas is lower due to multiple reflections off building walls that effectively "capture" more of the incoming solar radiation. The specified albedo needs to be compatible with the particular urban parameterization. For example, an area-average urban albedo will not be appropriate for a method that tries to incorporate wall reflection implicitly or that computes rooftop albedo separately.

Molecular Properties. Urban values for density, heat capacity, and thermal conductivity are needed to compute the ground flux in the surface energy balance. Values for specific building materials (e.g., steel, brick, concrete, asphalt) can be found in the literature (e.g., Oke[23]). However, in general, area-average values are needed that consider the fraction of urban and vegetated landuse within a grid cell, and the

Table 1. Urban Landuse Properties

	downtown/city center	industrial/commercial	residential
f_{urban}	0.8-1.0	0.9-1.0	0.5-0.7
f_{roof}	0.3-0.4	0.3-0.4	0.15-0.25
f_{cnyn}	est. 0.5-0.6	est. 0.6-0.7	0.15-0.4
h_c [m]	15-100's	5-25	5-15
Bowen ratio	1.5-∞	1.5-∞	0.5-1.0
urban albedo		0.10-0.27 (avg. 0.15)	
urban emissivity		0.85-0.96 (avg. 0.95)	
roof albedo		0.08-0.35	
roof emissivity		0.90-0.92	

representative fractions of building materials. Brown and Williams[62] have used ρ =2300 kg/m^3, C_p = 880 J/(kgK), and k = 1.2e-06 m^2/s for all urban land-use types in the surface energy budget balance. When converted to thermal admittance ($\rho C_p k^{1/2}$), these values fall within the 800-3000 range given by Oke (1987). One might consider having separate molecular property values for walls, roofs, and streets, for example, if the fractions of each within each grid cell can be determined.

Drag Coefficient. The drag force in the momentum eqn. (17) and the turbulent production term in the tke eqn. (21) are linearly dependent on the magnitude of the drag coefficient C_D. Hoerner[68] lists C_D values ranging from 0.7 to 1.5 for different size and shape buildings. Although there should be dependence on number, spacing, height, and shape of buildings, as well as approach flow angle, Brown and Williams[62] use an average value of 1.0 for all urban landuse categories. One might also expect that the drag coefficient will decrease in regions where buildings are closely spaced and the building heights are all about the same height, and increase when building heights change relative to one another. For comparison, Yamada[60] used a C_D = 0.2 for trees. Irvine et al.[93] and Shaw and Schumann[94] deduced values of 0.20 and 0.15, respectively, for forested areas.

Canopy Area Density. The height dependence of the drag force and turbulent kinetic energy production is controlled through the canopy area density term a(z). There are numerous measurements of a(z) for different

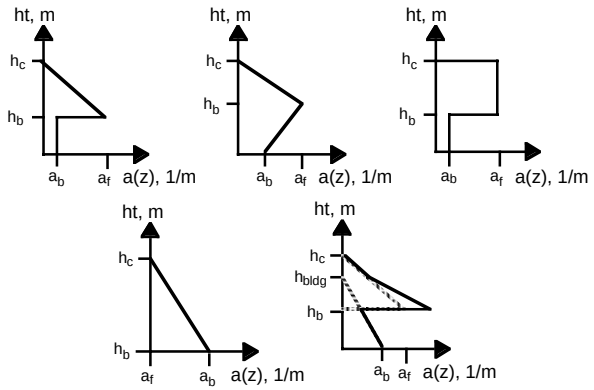

Figure 27. "Shape profiles" used for describing the canopy surface area density a(z) [m^2/m^3]. Four parameters are needed for describing the profiles: canopy height, base height, base surface area density, and foliage surface area density.

vegetative canopies (e.g., Arya [69], Watanabe and Kondo [95]), but we have not found a(z) profiles in the literature for the urban canopy. However, in earlier studies Brown and Williams[62] hypothesized a pyramid-shaped canopy area density profile for a mixed distribution of buildings (see Fig. 27). They use a mix of the pyramid and fir tree shapes for residential areas with mature trees which several authors have indicated may in fact be better described by a forest canopy (e.g., Oke[96]). The canopy area density profiles are described by analytical functions so that the cumulative canopy (leaf or building) area index eqn. (30) can be easily computed.

There clearly is a lot of uncertainty in the values of the above parameters. More analysis of urban datasets needs to be performed in order to better prescribe these parameters. In addition, high resolution modeling could be performed to determine some of the coefficients (e.g., the drag and extinction coefficients) as functions of building configuration, for example. Sensitivity tests, like those being done by Leach and Chen[97], need to be performed as well in order to determine what coefficients need to be specified more precisely.

4.2 Validation

One of the major difficulties in testing the urban canopy parameterizations is in the comparison of area-averaged model results to measurements that are typically representative of a point in space. From point-to-point within the urban environment, the local impact of buildings and landuse can vary dramatically. For example, the wind speed can be very strong on one street due to channeling, but on a side street be very weak and in the opposite direction due to street canyon vortex formation. Or, on the sunny side of a street overlying asphalt, the near-surface air temperature could be very warm, whereas on the opposite side of the street in the shade overlying a strip of vegetation the near-surface air temperature could be dramatically lower. Hence, individual measurements can be misleading when assessing the impact of the urban canopy and can prove difficult to use for model validation.

For urban canopy parameterization validation, field experiments need to be designed such that enough measurements are taken to properly represent an area average or sensors should be ideally placed to represent an upstream area rather than a local microscale feature. However, in practice this is difficult to do due to limited resources.

Another option is to numerically simulate at high resolution the fluid flow, thermodynamics, and/or surface energy budget around groups of buildings. For example, a detailed radiation balance could be performed using models of the type developed, for example, by Arnfeld[43] and Mills[46] and then area-averaged results could be obtained for different building configurations. Figure 28 shows the area-averaged flow field produced by a computational fluid dynamics model around a 3-d array of obstacles. Velocity profiles computed with a mesoscale model incorporating urban parameterization could then be compared to the CFD result in order to test, for example, the drag coefficient value.

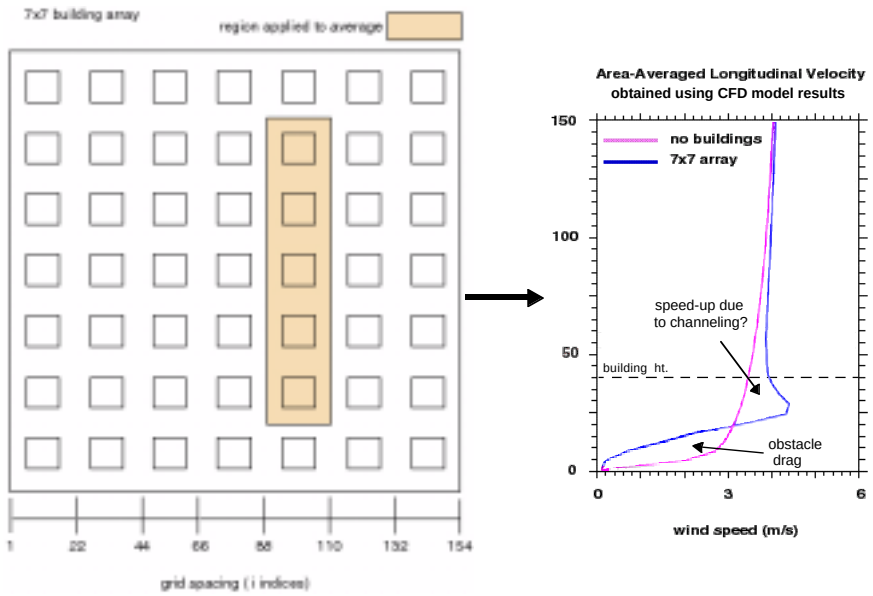

Figure 28. Top view of obstacle layout (left) and area-averaged velocity profiles computed by computational fluid dynamics model with and without obstacles (right) (Smith[98]).

5. Conclusions

Urban parameterizations developed for use in mesoscale meteorological models to account for the area-average effect of drag, turbulence production, heating, and surface energy budget modification induced by buildings and urban landuse have been described. It was shown that the city impacts the surface energy budget and the dynamic and thermodynamic flow fields. Urban areas are typically warmer than the surrounding country side at night and the heat island may result in thermodynamically-driven winds. The buildings in urban areas also create drag and produce turbulence, effectively changing the flow dynamics within and above the urban canopy. Being able to simulate these urban effects in mesoscale models is important for many applications.

Modifications to the surface energy budget and heat equation to account for urban influences were described, including approaches that accounted for radiation attenuation, anthropogenic heating, and urban surface properties. Drag and turbulence parameterizations with different levels of sophistication were covered as well, including the surface roughness, attenuation, and the drag coefficient approaches. It was argued that the traditional surface roughness approach is not appropriate for some applications, specifically when one is interested in computing the area-averaged flow fields within the urban canopy. The attenuation approaches were found suitable as a method for diagnostic wind models or vertically-coarse resolution prognostic simulations. Additional work, however, needs to be done in determining the coefficients for urban areas in order to make this approach practical. The drag coefficient approach was described as being useful for mesoscale modeling when the urban canopy layer is resolved by the model. In theory, it is capable of correctly simulating the area-average wind and tke profile variation with height within the canopy layer. The drawback to this approach is the number of parameters that need to be specified, some of which are not known with high precision. Uncertainties in parameter specification and difficulties with testing the parameterizations were covered. Future work using high resolution CFD and surface energy balance models was proposed in order to test the parameterizations and specify some of the parameters.

Acknowledgements. The author wishes to thank Mike Williams for insightful discussions on urban canopy parameterizations, Cathrin Muller for help with digitizing and plotting many of the figures, and Gerald Streit and Steven Burian for their editorial comments. This work was funded by the Department of Energy's Chemical and Biological Non-Proliferation Program.

References

[1] Bornstein, R., Mean diurnal circulation and thermodynamic evolution of urban boundary layers, *Modeling the Urban Boundary Layer*, Am. Met. Soc., Boston, 1987.

[2] Hosker, R., Flow and diffusion near obstacles, *Atmospheric Science and Power Production*, USDOE, 1984.

[3] Hanna, S. & Chang, J., Boundary-layer parameterizations for applied dispersion modeling over urban area, *Bound. Layer Meteor.*, **58**, pp. 229-259, 1992.

[4] Hanna, S., Ramsdell, J., & Cramer, H., Urban Gaussian diffusion parameters, *Modeling the Urban Boundary Layer*, Am. Met. Soc., Boston, 1987.

[5] Hosker, R., The effects of buildings on local dispersion, *Modeling the Urban Boundary Layer*, Am. Met. Soc., Boston, 1987.

[6] Yamartino, R., Strimaitis, D., & Messier, T., Modification of highway air pollution models for complex site geometries, vol. 1, Data analyses and development of the CPB-3 model, *Rep. No. FHWA-RD-89-112*, 1989.

[7] Brown, M. & Streit, G., Emergency Responders' 'Rules-of-Thumb' for Air Toxics Releases in Urban Environments, *Los Alamos Report LA-UR-98-4539*, 1999.

[8] Chandler, T., *The Climate of London*, Hutchison, London, 1968.

[9] Daigo, M. & Nagao, T., *Urban Climatology*, Asakura-Shoten, Tokyo, 214 pp., 1972.

[10] Landsberg, H., Inadvertent atmospheric modification through urbanification, *Weather and Climate Modification*, W. Hess, ed., John Wiley and Sons, New York, pp. 726-763, 1974.

[11] Oke, T., Review of Urban Climatology, 1969-1973, *WMO Publ. Tech. Note 134*, 132 pp., 1974.

[12] Bornstein, R., Observations of the urban heat island effect in New York City, *J. Appl. Meteor.*, **7**, pp. 575-582, 1968.

[13] Clarke, J., Nocturnal urban boundary layer over Cincinnati, Ohio, *Mon. Wea. Rev.*, **97**, pp. 582-589, 1969.

[14] Ludwig, F., Urban temperature fields, *WMO Publ. Tech. Note 108*, pp. 80-107, 1970.

[15] Oke, T. & East, C., The urban boundary layer in Montreal, *Bound.-Layer Meteor.*, **1**, pp. 411-437, 1971.
[16] Angel, J., Pack, D., Dickson, C., & Hoecker, W., Urban influence on nighttime airflow estimated from tetroon flights, *J. Appl. Meteor.*, **10**, pp. 194-204, 1971.
[17] Ackerman, B., METROMEX: Wind fields over the St. Louis metropolitan area, *Bull. Amer. Meteor. Soc.*, **55**, pp. 93-95, 1974.
[18] Myrup, L., A numerical model of the urban heat island, *J. Appl. Meteor.*, **8**, pp. 896-907, 1969.
[19] Atwater, M., Thermal effects of urbanization and industrialization in the boundary layer: a numerical study, *Bound.-Layer Meteor.*, **3**, pp. 229-245, 1972.
[20] McElroy, J., A numerical study of the nocturnal heat island over a medium-sized mid-latitude city (Columbus, Ohio), *Bound.-Layer Meteor.*, **3**, pp. 442-453, 1973.
[21] Bornstein, R., The two-dimensional URBMET urban boundary layer model, *J. Appl. Meteor.*, **14**, pp. 1459-1477, 1975.
[22] Oke, T., The surface energy budgets of urban areas, *Modeling the Urban Boundary Layer*, Am. Met. Soc., Boston, 1987.
[23] Oke, T., *Boundary-Layer Climates*, Routledge, London, 1987.
[24] Lowry, W., The climate of cities, *Scientific American*, 1967.
[25] Liu, J., Arya, S., Snyder, W., & Lawson, R., A laboratory simulation of turbulent convection over an urban heat island,
[26] Sahashi, K., Hieda, T., & Yamashita, E., Nitrogen-oxide layer over the urban heat island in Okayama City, *Atmos. Env.*, 30, pp. 531-535, 1996.
[27] Saitoh, S., Shimada, T., & Hoshi, H., Modeling and simulation of the Tokyo urban heat island, *Atmos. Env.*, **30**, pp. 3431-3442, 1996.
[28] Tapper, N., Urban influences on boundary layer temperature and humidity: results from Christchurch, New Zealand, *Atmos. Env.*, **24B**, pp. 19-27, 1990.
[29] Shreffler, J., Detection of centripetal heat-island circulations from tower data in St. Louis, *Bound.-Layer Meteor.*, **15**, pp. 229-242, 1978.
[30] Kuttler, W. and Romberg, E., The occurrence and effectiveness of country breezes by means of wind tunnel and in-situ measurements, *Proc. 9th World Clean Air Congr.*, Montreal, Quebec, 1992.

[31] Oke, T., Canyon geometry and the nocturnal urban heat island: comparison of scale model and field observations, *J. Climatol*., **1**, pp. 237-254, 1981.
[32] Oke, T. and Hannell, F., The form of the urban heat island in Hamilton, Canada, *Urban Climates, WMO Tech. Note 108*, pp. 113-126, 1970.
[33] Oke, T., The distinction between canopy and boundary layer urban heat islands, *Atmos.*, **14**, pp. 268-277, 1976.
[34] Hogstrom, U., Taesler, R., Karlsson, S., Enger, L., & Hogstrom, A., The Uppsala Urban Meteorology Project, *Bound.-Layer Meteor.*, **15**, pp. 69-80, 1978.
[35] Bowne, N. & Ball, J., Observation comparison of rural and urban boundary layer turbulence, *J. Appl. Meteor*., **9**, pp. 862-873, 1970.
[36] Godowitch, J., Characteristics of vertical turbulent velocities in the urban convective boundary layer, *Bound.-Layer Meteor*., **35**, pp. 387-407, 1986.
[37] Pendergrass, W. & Arya, S., Dispersion in neutral boundary layer over a step change in surface roughness – I. Mean flow and turbulence structure, *Atmos. Env.*, 18, pp. 1267-1279, 1984.
[38] Theurer, W., Baechlin, W., & Plate, E., Model study of the development of boundary layers above urban areas, *J. Wind Eng. & Ind. Aerodyn.*, **41-44**, pp 437-448, 1992.
[39] Brown, M., Lawson, R., DeCroix, D., & Lee R., Mean flow and turbulence measurements around a 2-d array of buildings in a wind tunnel, *11th AMS Appl. of Air Poll. Meteor. Conf.*, Long Beach, Ca., 2000.
[40] Roth, M., Vertical structure of turbulence over cities, *2nd AMS Urban Env. Symp*., Albuquerque, NM, 1998.
[41] Rotach, M., Profiles of turbulence statistics in and above and urban street canyon, *Atmos. Env*., **29**, pp. 1473-1486, 1995.
[42] Oikawa, S. & Meng, Y., A field study of diffusion around a model cube in a suburban area, *Bound.-Layer Meteor*., **84**, pp. 399-410, 1997.
[43] Arnfeld, A., An approach to the estimation of the surface radiative properties and radiation budgets of cities, *Phys. Geog.* **3**, pp. 97-122, 1982.

[44] Murakami, S., Current status and future trends in computational wind engineering, *J. Wind Eng. & Ind. Aerodyn.*, **67** & **68**, pp. 3-34, 1997.
[45] Oke, T., Johnson, G., Steyn, D., & Watson, I., Simulation of surface urban heat islands under "ideal" conditions at night, Part 2: Diagnosis of causation, *Bound.-Layer Meteor.*, **56**, pp. 339-358, 1991.
[46] Mills, G., An urban canopy-layer climate model, *Theor. Appl. Climatol*., **57**, pp. 229-244, 1997.
[47] Delage, Y. & Taylor, P., Numerical studies of heat island circulations, *Bound.-Layer Meteor*., **1**, pp. 201-226, 1970.
[48] Vukovich, F., Dunn, J., & Crissman, B., A theoretical study of the St. Louis heat island: the wind and temperature distribution, *J. Appl. Meteor*., **15**, pp. 417-440, 1976.
[49] Hjelmfelt, M., Numerical simulation of the effects of St. Louis in mesoscale boundary-layer airflow and vertical air motion: simulations of urban vs. non-urban effects, *J. Appl. Meteor.*, **21**, pp. 1239-1257, 1982.
[50] Schultz, P. & Warner, T., Characteristics of summertime circulations and pollutant ventilation in the Los Angeles basin, *J. Appl. Meteor*., **21**, pp. 672-682, 1982.
[51] Byun, D. & Arya, S., A two-dimensional mesoscale numerical model of an urban mixed layer - I. Model formulation, surface energy budget, and mixed layer dynamics, *Atmos. Env*., **24A**, pp. 829-844, 1990.
[52] Kimura, F. & Takahashi, S., The effects of land-use and anthropogenic heating on the surface temperature in the Tokyo metropolitan area: a numerical experiment, *Atmos. Env.*, **25B**, pp. 155-164, 1991.
[53] Mochida, A., Murakami, S., Ojima, T., Kim, S., Ooka, R., & Sugiyama, H., CFD analysis of mesoscale climate in the greater Tokyo area, *J. Wind Eng. Ind. Aerodyn.*, **67** & **68**, pp. 459-477, 1997.
[54] Carissimo, B., Numerical simulation of meteorological conditions for peak pollution in Paris, *22nd NATO/CCMS Conf.*, Clermont-Fernand, France, 1997.

[55] Kitada, T., Okamura, K., & Tanaka, S., Effects of topography and urbanization on local winds and thermal environment in the Nohbi Plain, coastal region of central Japan: a numerical analysis by mesoscale meteorological model with a k-ε turbulence model, *J. Appl. Meteor*., **37**, pp. 1026-1046.
[56] Hafner, J. & Kidder, S., Urban heat island modeling in conjunction with satellite-derived surface/soil parameters, *J. Appl. Meteor.*, **38**, pp. 448-465.
[57] Taha, H., Modifying a mesoscale meteorological model to better incorporate urban heat island storage: a bulk parameterization approach, *J. Appl. Meteor*., **38**, pp. 466-473.
[58] Perez-Garcia, I. & Nickerson, E., The applicability of a mesoscale model in the Valley of Mexico during extreme air pollution episodes, 1997.
[59] Sorbjan, Z. & Uliasz, M., Some numerical urban boundary-layer studies, *Bound.-Layer Meteor*., **22**, pp. 481-502, 1982.
[60] Yamada, T., A numerical study of turbulent airflow in and above a forest canopy, *J. Met . Soc. Japan*, **60**, 439-454, 1982.
[61] Williams, M., Brown, M., Cruz, X., Sosa, G. & Streit, G., Development and testing of meteorology and air dispersion models for Mexico City, *Atmos. Env*., **29**, pp. 2929-2960, 1995.
[62] Brown M. & Williams, M., An urban canopy parameterization for mesoscale meteorological models, *AMS 2nd Urban Env. Symp.*, Albuquerque, NM, 1998.
[63] Maruyama, T., Surface and inlet boundary conditions for the simulation of turbulent boundary layer over complex rough surfaces, *J. Wind. Eng. Ind. Aerodyn.*, **81**, pp. 311-322, 1999.
[64] Urano, A., Ichinose, T., & Hanaki, K., Thermal environment simulation for three dimensional replacement of urban activity, *J. Wind. Eng. Ind. Aerodyn*., **81**, pp. 197-210, 1999.
[65] Ca V., Asaeda, T., & Ashie, Y., Development of a numerical model for the evaluation of the urban thermal environment, *J. Wind Eng. Ind. Aerodyn*., **81**, pp. 181-196, 1999.
[66] Whitaker, S., *Introduction to Fluid Mechanics*, Robert Krieger Pub. Co., Malabar, FL, 1984.

[67] Panton, R., *Incompressible Flow*, John Wiley and Sons, New York, NY, 1984.
[68] Hoerner, S., *Fluid-Dynamic Drag*, self-published, Lib. Congress Cat Card #64-196666, 1965.
[69] Arya, S., *Introduction to Micrometeorology*, Academic Press, San Diego, CA, 1988.
[70] Plate, E., *Aerodynamic Characteristics of Atmospheric Boundary Layers*, AEC Critical Reviews, USDOE, TID-25465, 1971.
[71] Hall, D., McDonald, R., Walker, S., & Spanton, A., Measurements of dispersion within simulated urban arrays – a small scale wind tunnel study, *BRE Client Report CR 178/96*, Building Research Establishment, Garston, Watford, 1996.
[72] Letau, H., Note on aerodynamic roughness parameter estimation on the basis of roughness element description, *J. Appl. Meteor.*, **8**, pp. 828-832, 1969.
[73] Raupach, M., Drag and drag partition on rough surfaces, *Bound.-Layer Meteor.*, **60**, pp. 375-395, 1992.
[74] Bottema, M., Urban roughness modelling in relation to pollutant dispersion, *Atmos. Env.*, **31**, pp. 3059-3075, 1997.
[75] McDonald, R., Griffiths, R., & Hall, D., An improved method for the estimation of surface roughness of obstacle arrays, *Atmos. Env.*, **32**, pp. 1857-1864, 1998.
[76] Duijm, N., Estimates of roughness parameters for arrays of obstacles, Bound.-Layer Meteor., 91,
[77] Grimmond, S. & Oke, T., Urban roughness parameters: morphometric analysis, *12th AMS Symp. Bound. Layers & Turb.*, Vancouver, BC, 1997.
[78] Cionco, R., A wind-profile index for canopy flow, *Bound.-Layer Meteor.*, **3**, pp. 255-263, 1972.
[79] Pielke, R., *Mesoscale Meteorological Modeling*, Academic Press, San Diego, CA, 1994.
[80] Cionco, R. & Ellefsen, R., High resolution urban morphology data for urban wind flow modeling, *Atmos. Env.*, **32**, pp. 7-17, 1998.
[81] Wilson, N. & Shaw, R., A higher order closure model for canopy flow, *J. Appl. Meteor.*, **16**, pp. 1197-1205, 1977.

[82] Liu, J., Chen, J., Black, T. & Novak, M., E-e modeling of turbulent airflow downwind of a model forest edge, *Bound.-Layer Meteor*. **77**, 21-44, 1996.

[83] Hirt, C., Volume-fraction techniques: powerful tools for wind engineering, *1st Int. Symp. Comp. Wind Eng.*, Tokyo, 1992.

[84] Ingram, D., Batten, P., Causon, D., & Saunders, R., The representation of small scale obstructions in hydrocode calculations, from *Flow and Dispersion through Groups of Obstacles*, Clarendon Press, Oxford, 1997.

[85] Bottema, M. & Sini, J., Intercomparison and validation of different numerical approaches for simulating flow near urban roughness changes, *EACWE*, Genova, Italy, 1997.

[86] Brown, M. & Muller, C., The effect of microscale urban canyon flow on mesoscale puff dispersion, *AMS 12th Symp. Bound. Layers & Turb*., Vancouver, BC, 1997.

[87] Rotach, M., The turbulence structure in an urban roughness sublayer, from *Flow and Dispersion through Groups of Obstacles*, Clarendon Press, Oxford, 1997.

[88] Ayotte, K, Finnigan, J., Raupach, M., A second-order closure for neutrally stratified vegetative canopy flows, *Bound.-Layer Meteor.*, **90**, pp. 189-216, 1999.

[89] Yoshida, A. & Kunitomo, T., One-dimensional simulation of the thermal structure of urban atmospheres, *Int. J. Heat Mass Transfer*, **29**, pp. 1041-1049, 1986.

[90] Voogt, J. & Oke, T., Complete urban surface temperatures, *J. Appl. Meteor.*, **36**, pp. 1117-1132, 1997.

[91] Brown, M. & Williams, M., The effect of urban canopy parameterizations on mesoscale meteorological model simulations in the Paso del Norte area, *AWMA 90th Ann. Conf.*, Toronto, 1997.

[92] Grimmond, S., Cleugh, H., & Oke, T., An objective urban heat storage model and its comparison with other schemes, *Atmos. Env.*, **25B**, pp. 311-326, 1991.

[93] Irvine, M., Gardiner, B. & Hill, M., The evolution of turbulence across a forest edge, *Bound.-Layer Meteor*. **84**, 467-496, 1997.

[94] Shaw, R. & Schumann, U., Large-eddy simulation of turbulent flow above and within a forest, *Bound.-Layer Meteor*. **61**, pp. 47-64, 1992.
[95] Watanabe, T. & Kondo, J., The influence of canopy structure and density upon the mixing length within and above vegetation, *J. Met. Soc. Japan*, **68**, 227-235, 1990.
[96] Oke, T., The micrometeorology of the urban forest, *Phil. Trans. R. Soc. Lond. B*, **324**, pp. 335-349, 1989.
[97] Leach, M. & Chen, S., personal communication, 1999.
[98] Smith, S., personal communication, 1999.